

THE DIFFUSION CONTROLLED REACTION

BETWEEN MgO and β - QUARTZ

THE DIFFUSION CONTROLLED REACTION

BETWEEN MgO AND β - QUARTZ

by

JOHN GEORGE LENZ, B. Sc.

A Thesis

Submitted to the School of Graduate Studies

in Partial Fulfilment of the Requirements

for the Degree

Master of Science

McMaster University

February 1975

MASTER OF SCIENCE (1975)
(Material Science)

McMASTER UNIVERSITY
Hamilton, Ontario

TITLE: The Diffusion Controlled Reaction Between MgO and
 β - Quartz.

AUTHOR: John George Lenz, B. Sc. (University of Calgary,
Calgary Alberta)

SUPERVISOR: Dr. P. S. Nicholson

NUMBER OF PAGES: xi, 93

SCOPE AND CONTENTS

This thesis is concerned with the investigation of the diffusion controlled reaction between MgO and β - quartz in the temperature range 1200 - 1450 °C in wet and dry atmospheres. The reactions were studied by placing known faces of quartz crystals in direct contact with MgO powder, heat treating them, and then investigating the cross sections. The product layer was investigated by both reflected light and thin section metallography, electron - microprobe and X- ray diffraction. Using Wagner's and Schmalzried's ideas on solid state reactions, a theoretical model for the diffusion controlled formation of silicates was developed. With this model, a mechanism for the diffusion controlled formation of forsterite from MgO and β - quartz was advanced.

ACKNOWLEDGMENTS

I would like to thank my supervisor, Dr. P. S. Nicholson, for suggesting the problem and for offering guidance and encouragement in seeing the work to completion. I wish to especially thank Dr. W. W. Smeltzer for his helpful discussions and aid in clarifying the theory of solid state reactions. I am also indebted to many of the faculty, technical staff and my fellow graduate students for their aid in this work. Finally I would like to thank my wife, Dorothy, who not only typed the thesis and showed great patience, but also gave this work a purpose.

I gratefully acknowledge the financial support given by the National Research Council of Canada, in the form of a grant to Dr. Nicholson, and the Steel Company of Canada, in the form of a graduate student fellowship.

TABLE OF CONTENTS

	<u>Page</u>
CHAPTER I INTRODUCTION	1
CHAPTER II LITERATURE REVIEW	2
II.1 The System MgO - SiO ₂	2
II.2 Silica	4
II.3 Magnesium Oxide	11
II.4 Forsterite	11
II.5 Enstatite	13
II.6 Defect Structure of Forsterite	15
II.7 Review of Previous Work on the Reaction Between MgO - SiO ₂	21
II.7-1 Reaction Kinetics in the System MgO - SiO ₂	21
II.7-2 Thermodynamic Data for the System MgO - SiO ₂	25
II.8 Review of Solid State Reaction Kinetics	27
CHAPTER III EXPERIMENTAL WORK	36
III.1 Introduction	36
III.2 Sample Preparation	36
III.2-1 Starting Materials	36
III.2-2 Preparation of Reaction Samples	37
III.2-3 Apparatus	37
III.2-4 Experimental Procedure	39
III.2-5 Optical Examination	40
III.2-6 Electron Microprobe Measurements	40
III.2-7 X - ray Diffraction	41
CHAPTER IV RESULTS AND DISCUSSION	43
IV.1 Morphology and Composition of Reaction Product	43
IV.2 Kinetic Data	54

	<u>Page</u>
IV.3 The Reaction Mechanism	66
CHAPTER V SUGGESTIONS FOR FUTURE WORK	79
CHAPTER VI CONCLUSIONS	81
APPENDIX I KRÖGER - VINK DIAGRAM FOR FORSTERITE	83
APPENDIX II PREPARATION OF FORSTERITE AND ENSTATITE	86
APPENDIX III DIFFRACTION PATTERN OF PROTOENSTATITE	87
APPENDIX IV FURTHER THOUGHTS ON THE LACK OF ANISOTROPY OF THE REACTION AND ON THE EXISTENCE OF AN ENSTATITE LAYER BETWEEN THE QUARTZ AND FORSTERITE PHASES	88
REFERENCES	90

LIST OF ILLUSTRATIONS

<u>Figure</u>	<u>Subject</u>	<u>Page</u>
II-1	Binary Phase Diagram for the System $MgO - SiO_2$.	3
II-2a	Structure of α -Quartz Projected on (0001) Plane.	5
II-2b	Structure of β -Quartz Projected on (0001) Plane.	6
II-2c	The Structure of β - Tridymite.	7
II-2d	The Structure of β - Cristobalite	8
II-3	The Diffusion Coefficients of ^{22}Na parallel and Perpendicular to the C - axis of Quartz, and the Diffusion Coefficients of ^{45}Ca parallel to the C - axis of Quartz.	10
II-4	The Percentage of (-100+120) and (-240+300) Mesh Madagascar Quartz Remaining After Firing at 1320 °C and 1370 °C.	12
II-5	Olivine Structure Parallel to (100) Plane.	14
II-6	The Structure of a) Clino - enstatite, b) Enstatite and c) Proto - enstatite Projected on the (010) Plane.	16
II-7	Kröger - Vink Diagram for Mg_2SiO_4 .	19
II-8	Formation of Forsterite Expressed as a Percentage, from 13μ Cristobalite Particles in Fine - Grained MgO Matrix.	23
II-9	Formation of Forsterite by 14μ MgO Particles in a Matrix of Mixed Sizes Quartz Powder.	24
III-1	The Position of the Reacted Quartz Pellet in the Debye - Scherrer Camera.	42
IV-1	The Quartz - MgO Reaction Interface After Heating	44

<u>Figure</u>	<u>Subject</u>	<u>Page</u>
	at 1250 °C for 48 Hours.	
IV-2	A Quartz - MgO Reaction Couple Heated at 1340 °C for 24 Hours.	45
IV-3a	The Reaction Interface on the Prism Plane of Quartz After Heating at 1340 °C for 24 Hours.	46
IV-3b	The Reaction Interface on the Basal Plane of Quartz After Heating at 1340 °C for 24 Hours.	47
IV-4	Thin Section Micrograph of MgO - Quartz Reaction Interface on Basal Plane of Quartz Taken Under Crossed Nicols.	49
IV-5	Point Counts from an Electron Probe Scan Across the MgO - Quartz Interface.	50
IV-6a	The Debye - Scherrer Pattern Taken of the Quartz Pellet After Reacting with MgO at 1340 °C for 24 Hours.	52
IV-6b	The Debye - Scherrer Pattern Taken of the Quartz Pellet After Reacting with MgO at 1450 °C for 24 Hours.	52
IV-7	The Growth of Mg_2SiO_4 at 1203 °C on Both the Basal and Prism Planes of Quartz.	55
IV-8	The Growth of Mg_2SiO_4 on Both the Basal and Prism Planes of Quartz at 1245 °C.	56
IV-9	The Growth of Mg_2SiO_4 on Both the Basal and Prism Planes of Quartz at 1292 °C.	57
IV-10	The Growth of Mg_2SiO_4 on Both the Basal and Prism Planes at 1349 °C.	58
IV-11	The Growth of Mg_2SiO_4 on the Basal and Prism Planes of Quartz at 1415 °C.	59

<u>Figure</u>	<u>Subject</u>	<u>Page</u>
IV-12	The Rate of Growth of Mg_2SiO_4 in Atmospheres Containing 45, 135, 250 mm Hg Water Partial Compared with the Rate of Growth in Dry Atmospheres.	60
IV-13	The Plot of log Product Layer Thickness Versus log Time for the Growth of Mg_2SiO_4 at 1203, 1245, 1292, 1349, and 1415 °C.	63
IV-14	Plot of log Product Layer Thickness Versus log Time at 1200 °C with 45, 135, and 250 mm Hg Water Vapor Pressure.	64
IV-15	Activation Energy Plots for Reaction in the $MgO - SiO_2$ System.	68
IV-16	The Anisotropy of Ca_2SiO_4 Growth on the Basal and Prism Planes of Quartz in Dry and Wet Nitrogen Atmospheres.	71
IV-17	The Diffusivities of Mg^{2+} and O^{2-} in Mg_2SiO_4 Under Various Conditions.	76
IV-18a	A Possible Mechanism for the Incorporation of Interstitial Water in the Olivine Structure.	78
IV-18b	The Mechanism of Incorporation of Interstitial Water in Pure Silica.	78

LIST OF TABLES

<u>Table</u>	<u>Title</u>	<u>Page</u>
II-1	The Ionized Point Defects in Forsterite and the Probable Defect Types.	17
II-2	The Possible Reaction Mechanisms for the Solid State Reaction $2\text{MgO} + \text{SiO}_2 \rightarrow \text{Mg}_2\text{SiO}_4$.	29
IV-1	Debye - Scherrer X-ray Patterns Obtained from Couples Reacted at 1340 °C and 1450 °C for 24 Hours.	53
IV-2	Parabolic Data for the Reaction Between $\text{MgO} - \text{SiO}_2$.	61
IV-3	Slopes of the log - log Plots for the Reaction Between β - Quartz - MgO.	65
IV-4	Diffusion Coefficients of the Rate Controlling Species.	70

List of Symbols Used in Thesis

- D_i : self diffusion coefficient of i , where i is any ion or vacancy.
- E : electromotive force of a cell.
- F : Faraday's constant.
- ΔG° : free energy change of a reaction.
- K : reaction rate constant of the Ginstling - Brounshtein equation.
- K_j : equilibrium constant for reaction j .
- R : ideal gas constant.
- \underline{R} : particle radius of reactents.
- T : temperature, in degrees K unless otherwise stated.
- V : volume of product formed per equivalent of reactent transported across product layer.
- a_i : activity of component i .
- c_i : equivalent concentration of component i .
- i : symbol for any ion or vacancy which exists as a defect.
- j_i : flux of a species i .
- K_p : parabolic rate constant.
- n_i : characteristic number for each defect type, i .
- q : cross sectional area of reaction zone.
- t : reaction time.
- x : product layer thickness
- x_0 : product layer thickness extrapolated to $t \rightarrow 0$.
- z : valence of transport ion.
- z_i : absolute charge of i .
- α : fraction of total material which has reacted.
- γ : a dimensionless factor, dependent on the reaction mechanism.
- $\hat{\eta}$: the equivalent flux across the reaction layer of cross sectional

area, q , per unit time.

$\tilde{\mu}_i$: electrochemical potential per equivalent i .

CHAPTER I

INTRODUCTION

High temperature solid state reactions in ceramic systems are extremely important in many fields of technology, yet for the most part, little is known about the mechanisms of such reactions. The system MgO-SiO₂ for example is of prime importance in the field of refractories. Early workers^(1,2,3) in this system were primarily interested in determining which binary compounds form on reaction, and how these compounds affect the properties of refractory materials containing MgO and SiO₂. Initial efforts to obtain high temperature kinetic data^(4,5,6,7) in this system were carried out on mixed powders of MgO and SiO₂. Although this method gives data with a minimum expenditure of time and effort, it yields only empirical results, since reaction rates depend greatly on the size and shape of the reactant particles. In order to obtain meaningful data, it is necessary to carry out the reaction under well defined geometric and thermodynamic conditions. The kinetic data so obtained can be interpreted using the available theories of solid-state reactions so yielding a higher degree of understanding of the reaction mechanism.

CHAPTER II

LITERATURE REVIEW

II.I The System MgO-SiO₂

The system MgO-SiO₂ was initially studied by Bowen and Andersen⁽¹⁾ and by Greig⁽²⁾. By heating mixtures of MgO and SiO₂ in large electric arc furnaces, they determined that only two binary compounds form in this system; forsterite, Mg₂SiO₄ and enstatite, MgSiO₃. Forsterite was found to melt congruently at 1890 °C, whereas enstatite decomposed at 1557 °C to form a liquid and forsterite. The above workers believed clino - enstatite to be the stable high temperature form of enstatite, but subsequent work by Foster⁽¹⁵⁾ and Atlas⁽¹⁶⁾ has shown that proto - enstatite is the stable high temperature form, and that clino - enstatite is a metastable polymorph. The phase diagram of the MgO-SiO₂ system given in Figure II-1 is the one given by Greig, with the modifications of Foster and Atlas.

Schaudt and Roy⁽⁸⁾ have shown that there is a small degree of solid solubility in this system. Samples of forsterite with an MgO excess, and samples of MgO with forsterite were rapidly quenched from the annealing temperatures. At 1860 °C (the eutectic temperature of MgO - Mg₂SiO₄) the solubility of MgO in forsterite is approximately 0.5 mole %, and 11.0 mole % of forsterite can be dissolved in the MgO phase. Extrapolation of their results to lower temperatures predict that there is little solid solubility of MgO in the forsterite phase below 1600 °C. The solid solubility limits for the silica rich side of forsterite, and of enstatite have not been

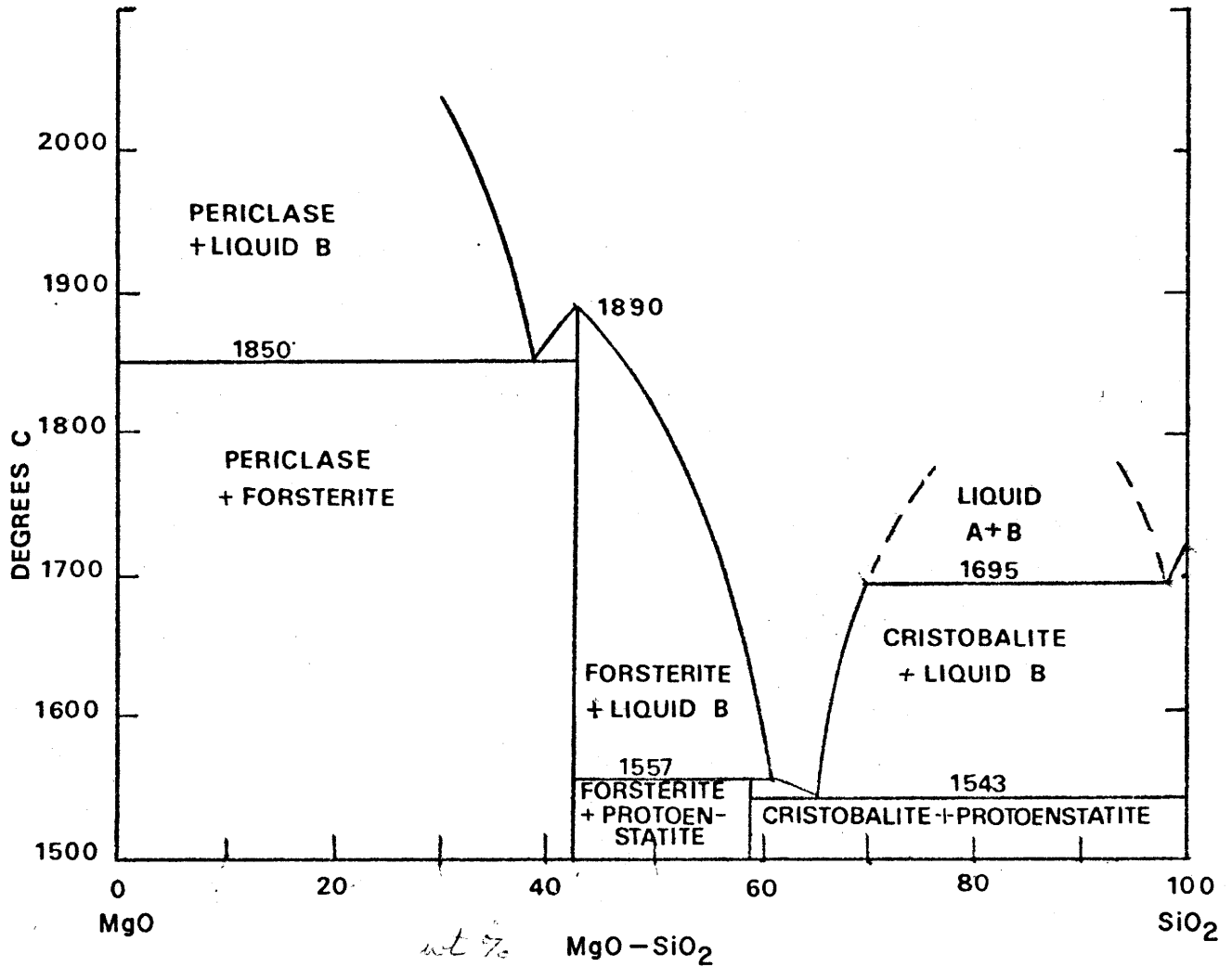


Figure II-1 Binary Phase Diagram for the System $\text{MgO} - \text{SiO}_2$.
 Based on diagram of Bowen and Anderson⁽¹⁾, and Greig⁽²⁾. The designation of the enstatite phases was modified to conform with the findings of Foster⁽¹⁵⁾ and Atlas⁽¹⁶⁾.

determined.

II.2 Silica (SiO₂)

Silica can exist in three stable polymorphs between room temperature and the melting point, 1760 °C, at standard pressure. These are quartz (stable up to 870 °C), tridymite (stable between 870 °C to 1470 °C), and cristobalite (stable from 1470 °C to the melting point). The structures of these polymorphs are shown in Figures II-2a to II-2d. In addition to these stable forms, silica can exist in a number of metastable forms. These are the amorphous state, silica W, a light chain structure of SiO₂, and three high pressure forms, coesite, keatite, and stishovite.

The structure of all crystalline forms of silica, and of silicates as well, is based on the SiO₄⁴⁻ tetrahedron. These tetrahedra may be regular or distorted and the oxygen at the apex may be shared by two tetrahedra. The structure of β-quartz is a three dimensional network formed of silica tetrahedra arranged along a hexagonal screw axis parallel to the C axis in a double helical fashion. Successive tetrahedra on the hexagonal chains are translated through C/3 as they undergo 1/6 rotation⁽¹¹⁾. Denser α-quartz forms through a displacive collapse of the silica tetrahedra.

The difference in thermal expansion between α + β quartz is quite marked. α-quartz has a thermal expansion coefficient of $150 \times 10^{-7} / ^\circ\text{C}$ while β-quartz has a slightly negative expansion coefficient of $-5 \times 10^{-7} / ^\circ\text{C}$ in its stability range⁽¹²⁾.

β-quartz will form a series of solid solutions with compounds such as MgAl₂O₄ and LiAlO₂. These "stuffed quartz" structures form by

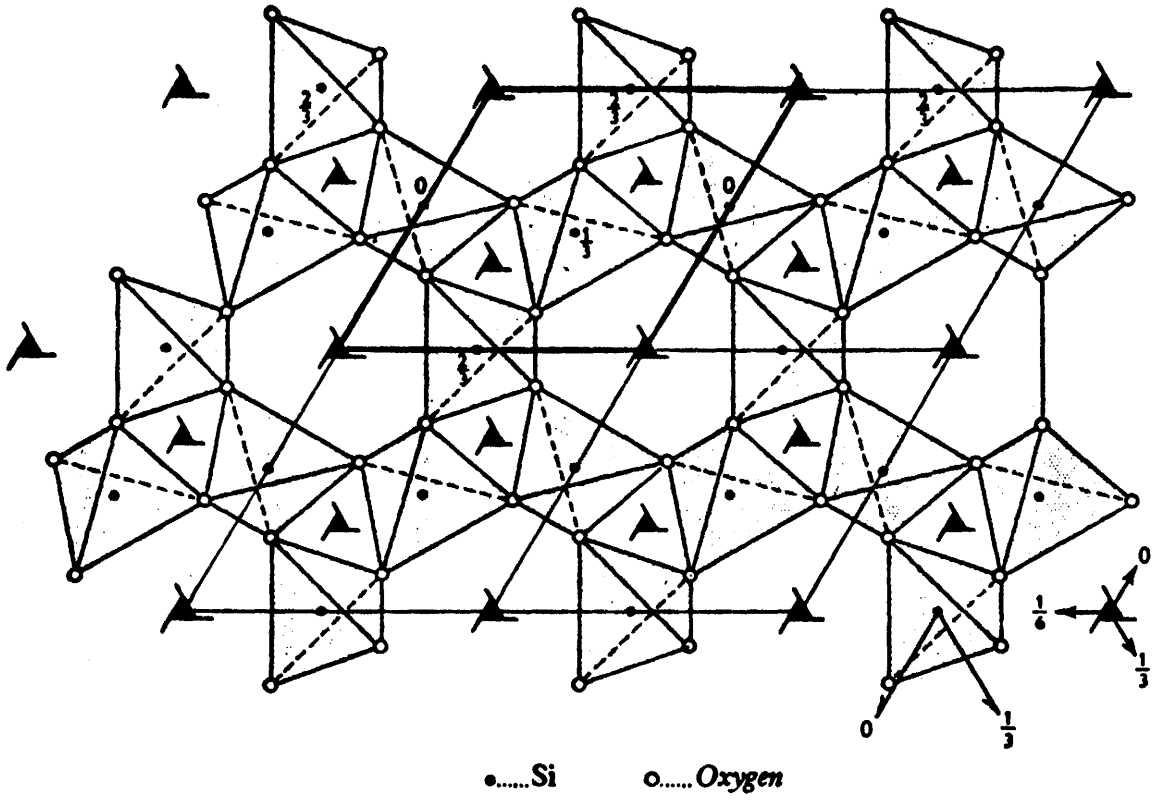


Figure II-2a Structure of α - quartz projected on (0001) plane after Wei⁽⁴⁶⁾.

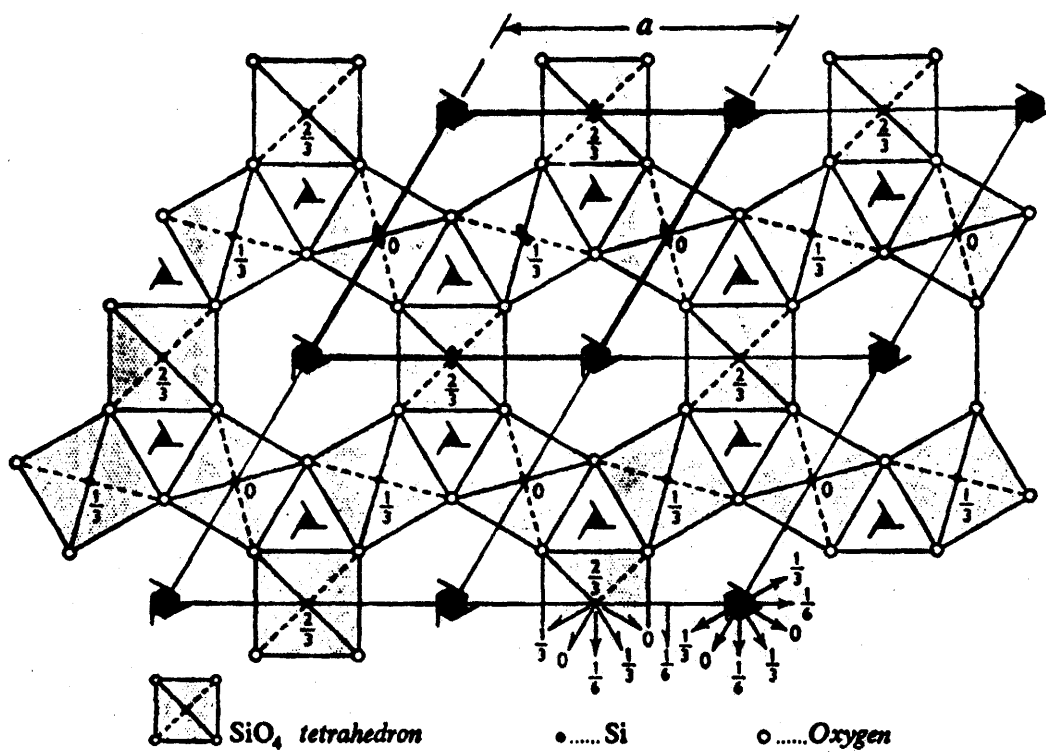


Figure II-2b The structure of β - quartz projected on (0001) plane, after Wychoff⁽⁴⁵⁾.

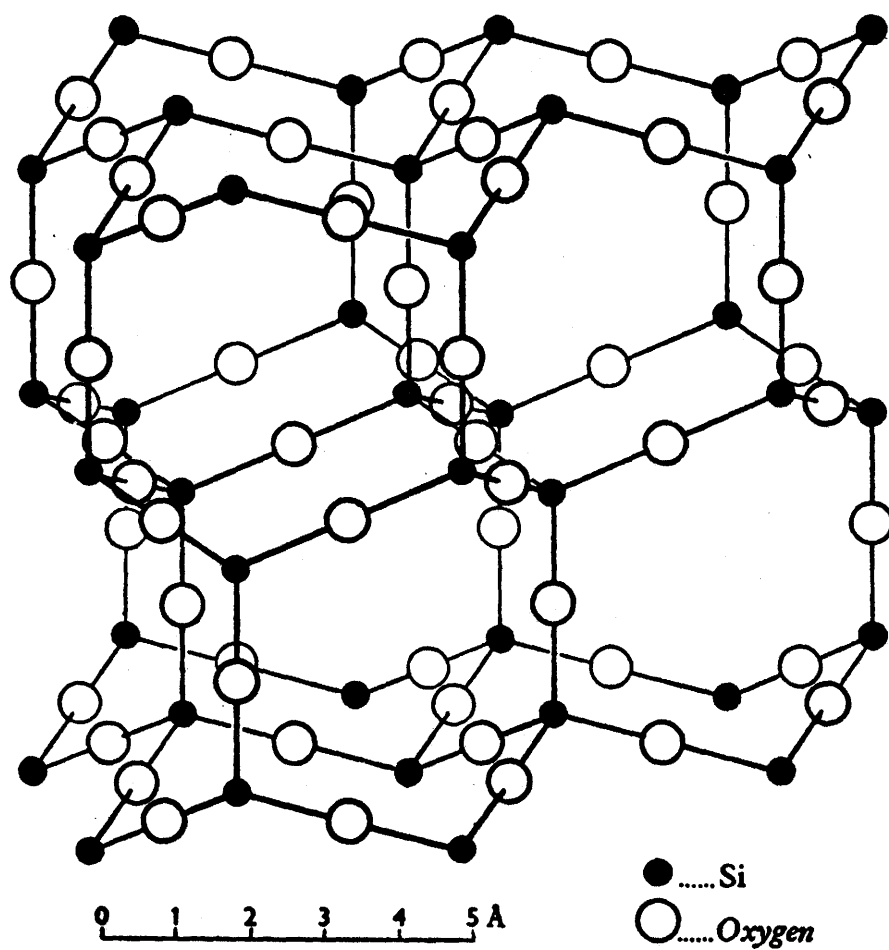


Figure II-2c The structure of β - tridymite, after W.L. Bragg⁽⁴⁷⁾.

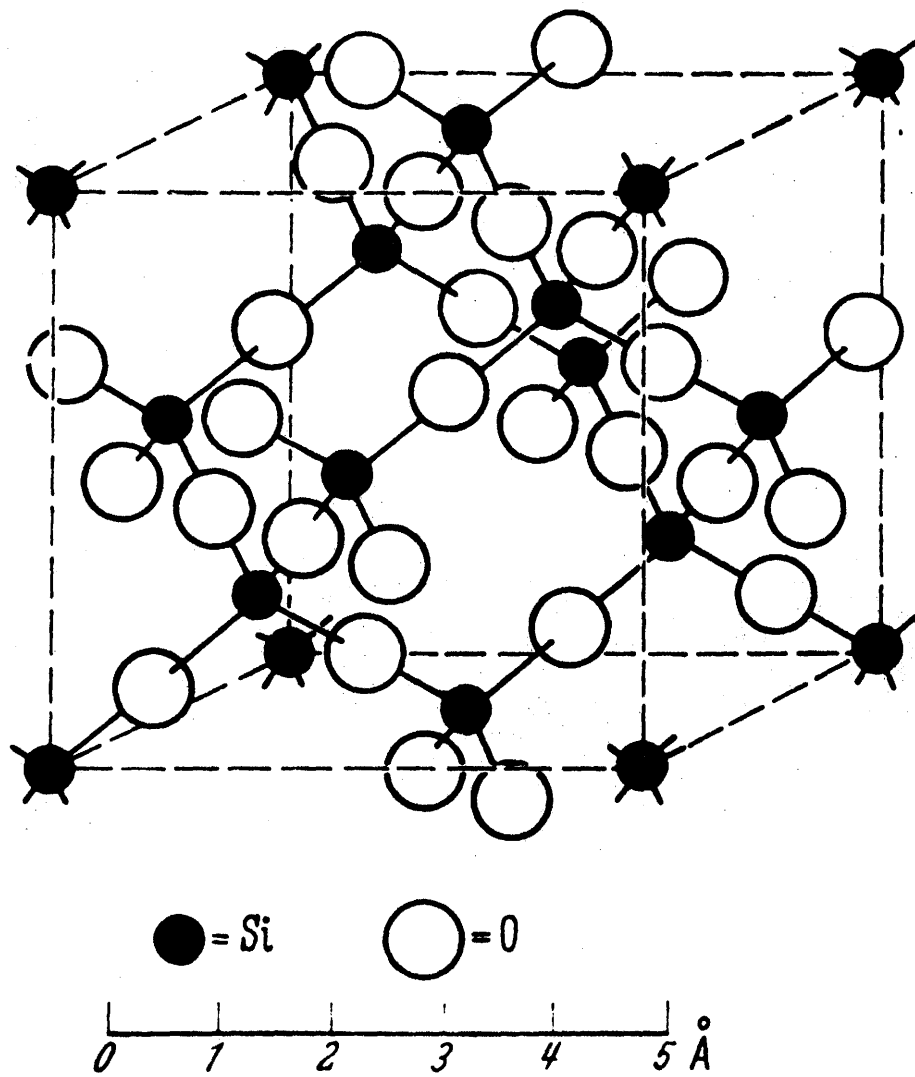


Figure II-2d The structure of β -cristobalite.

substitution of Al^{3+} for Si^{4+} , accompanied by either Mg^{2+} or Li^+ in the interstitial vacancy sites along the hexagonal screw axis. There is no indication however, that β - quartz will form a solid solution with MgO alone⁽¹²⁾.

Frischat^(13,14) has noted that there is a difference in the diffusion rates of radioactive $^{22}\text{Na}^+$ in quartz parallel to the C axis and perpendicular to the C axis. He found that Na^+ diffusion parallel to the C axis can be described by the equation $D = 0.68 \exp(-20,000/RT) \text{ cm}^2/\text{sec}$ in the temperature range 300 °C to 570 °C, while diffusion perpendicular to the C axis was three to four orders of magnitude lower. Frischat also measured the diffusion of $^{45}\text{Ca}^{2+}$ in quartz. The rate of Ca^{2+} diffusion parallel to the C axis can be described by $D = 1. \times 10^5 \exp(68,000/RT) \text{ cm}^2/\text{sec}$ whereas the diffusion perpendicular to the C axis was too low to be measured. His results are shown in Figure II-3. This anisotropy of ionic diffusion in quartz may cause differences in reaction rates on the basal and prism planes of quartz when involved in a reaction with a diffusing ionic species. If a rate determining step, or a nucleation step involves the diffusion of ionic species into quartz, anisotropy of reaction rates on different planes of quartz may also be expected. Burte and Nicholson^(25,51) have suggested that this effect may be the cause of the anisotropy of the reaction between β - quartz and CaO . It was found that the rate of formation of Ca_2SiO_4 was significantly greater on the basal plane (i.e. reaction parallel to the C axis) than on the prism plane (i.e. reaction perpendicular to the C axis) of β - quartz.

Heating quartz in the temperature range 870 °C - 1470 °C does not induce direct conversion to tridymite, but instead β - cristobalite forms⁽⁹⁾, which slowly converts to tridymite in the presence of an alkali mineralizer.

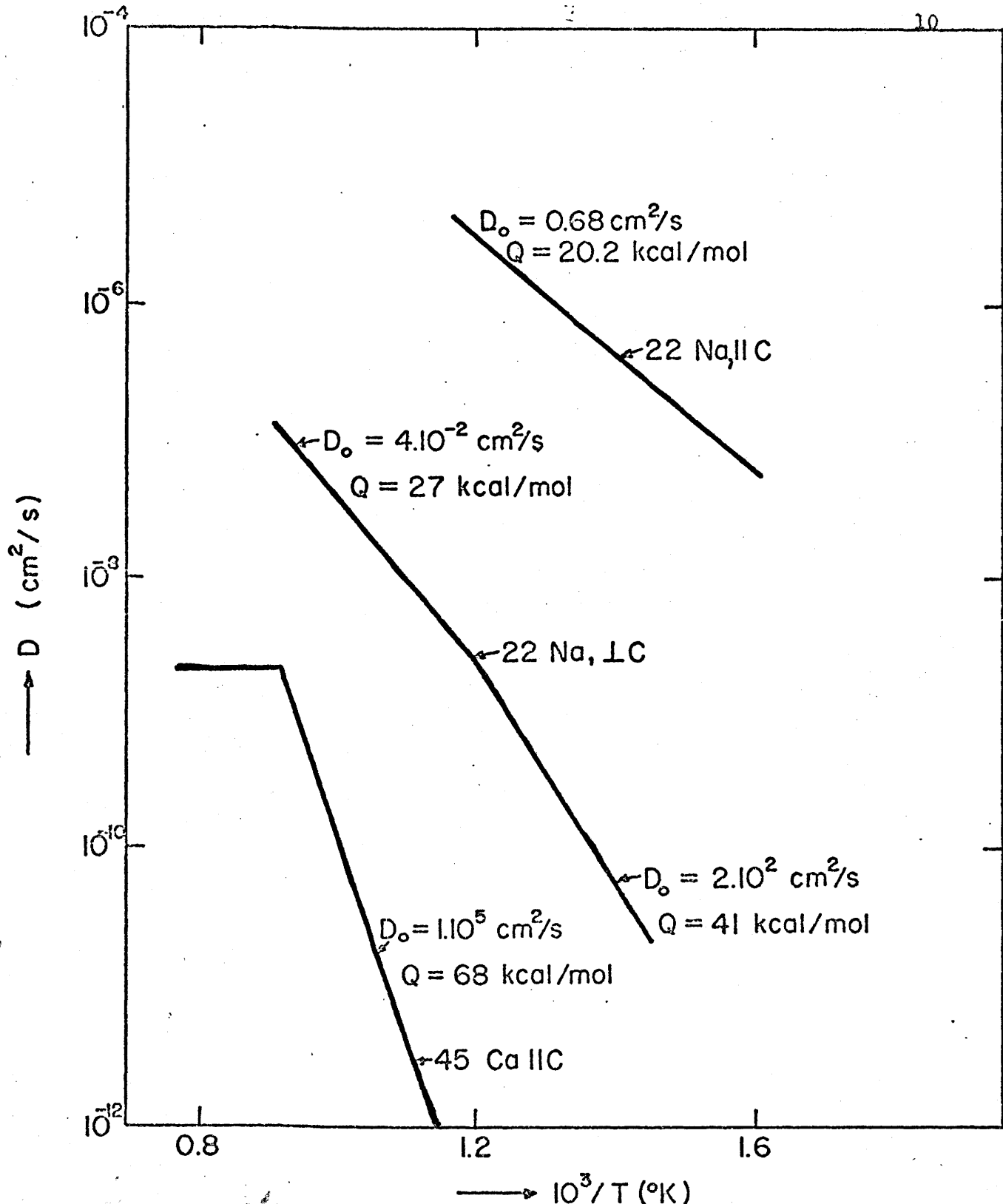


Figure II-3 The diffusion coefficients of ^{22}Na parallel and perpendicular to the C - axis of quartz, and the diffusion coefficient of ^{45}Ca parallel to the C - axis of quartz, according to Frischat^(13,14,50).

The rate of conversion of β - quartz to cristobalite has been studied in the temperature range 1270 °C to 1450 °C⁽¹⁰⁾ and it was found that the reaction is not simple first order, and that the rate of transformation depends on the particle size of quartz. Figure II-4 shows the dependence on particle size of the quartz - cristobalite transformation at 1320 °C and 1370 °C. The transformation is not a rapid one, for example, heating (-100 +125) mesh quartz particles at 1370 °C showed 93% to remain after 24 hours. The product phase is found to nucleate on surfaces, defects, and inclusions within the quartz, thus, large grain defect free quartz will have even a slower rate of transformation⁽¹⁰⁾. It has also been noted that MgO, CaO, TiO₂, and Fe₂O₃ mineralize the transformation of quartz to cristobalite.

In addition to the polymorphic changes in silica, high - low inversions also occur. These inversions involve changes in the Si-O-Si bond angles and do not require the Si-O-Si bonds to break. These high - low inversions occur in all three stable forms of silica, the most important one being the α - β quartz transition.

II.3 Magnesium Oxide (MgO)

Magnesium oxide is an ionic compound with the oxygen anions packed in a face centered cubic array and the magnesium cations filling all the available octahedral sites (NaCl structure). The melting point of MgO is given as 2800 °C⁽⁴⁰⁾. Only one polymorphic form of MgO is known.

II.4 Forsterite - Mg₂SiO₄

The mineral forsterite belongs to the olivine group. It is made

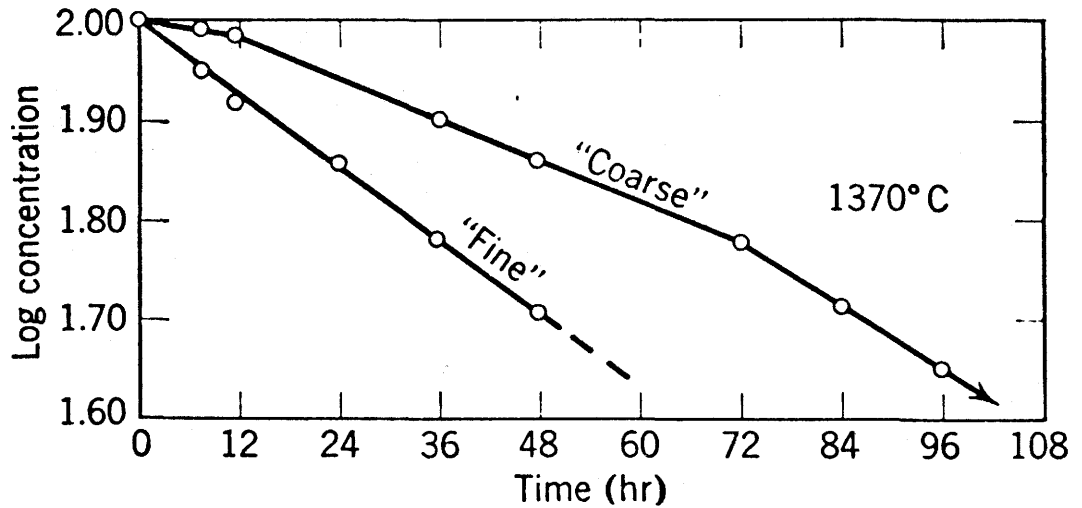
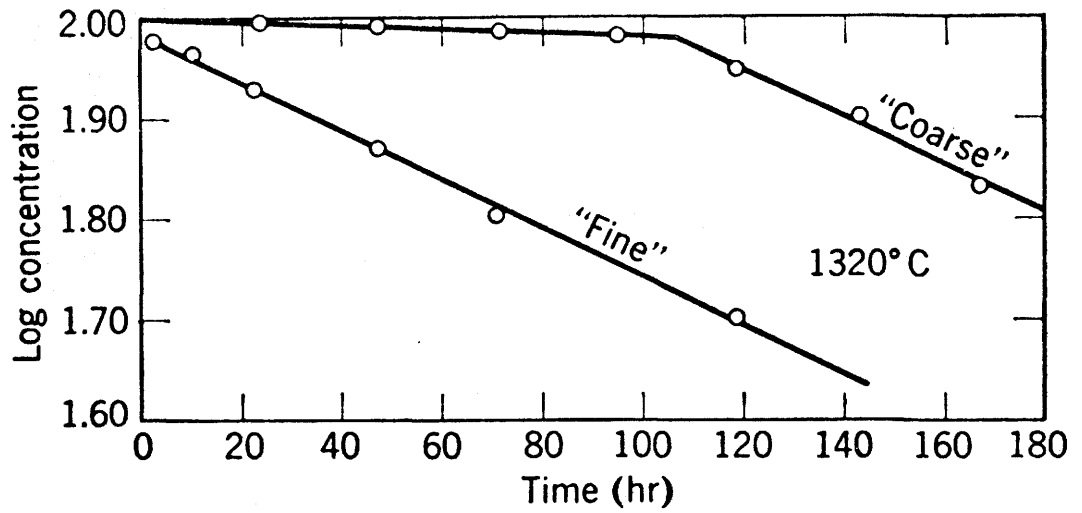


Figure II-4 The percentage of (-100 +120) and (-240 +300) mesh Madagascar quartz remaining after firing at 1320 °C and 1370 °C.

of isolated SiO_4^{4-} tetrahedra with magnesium cations balancing the charge. The oxygens are arranged to form an orthorhombic structure, with one - eighth of the tetrahedral sites filled with silicon cations, and one half of the octahedral sites filled with magnesium cations. At standard pressure, the orthorhombic structure is the only stable form of forsterite at all temperatures to its melting point. Two high pressure forms of forsterite also exist⁽⁵²⁾. These are β - Mg_2SiO_4 , which has a slightly distorted spinel structure, and γ - Mg_2SiO_4 , with a perfect spinel (cubic) structure. Suito⁽⁵²⁾ has found that at 1000 °C the olivine forsterite will transform to the β - Mg_2SiO_4 at approximately 130 kilo bar pressure, and a further transition to γ - Mg_2SiO_4 takes place at 220 kilo bar pressure. Similar olivine to spinel transformations are known to occur in other orthosilicates such as Ni_2SiO_4 , Co_2SiO_4 , and Fe_2SiO_4 .

II.5 Enstatite - MgSiO_3

The mineral enstatite is a chain silicate of the pyroxene group. It consists of repeat units of $(\text{Si}_2\text{O}_6)^{-2n}$ with magnesium cations to balance the charge. There are three known polymorphs of enstatite, however the relationship between these phases is not clear. Enstatite, with an orthorhombic crystal structure, is the stable low temperature form. Proto - enstatite, also with an orthorhombic structure, is a high temperature form stable above 1260 °C according to Foster⁽¹⁵⁾ or 985 °C according to Atlas⁽¹⁶⁾. Monoclinic clino - enstatite is a metastable form formed by rapid cooling of proto - enstatite below 700 °C^(15,16). Clino - enstatite can exist indefinitely at room temperature without reverting to enstatite⁽¹⁵⁾. Structures

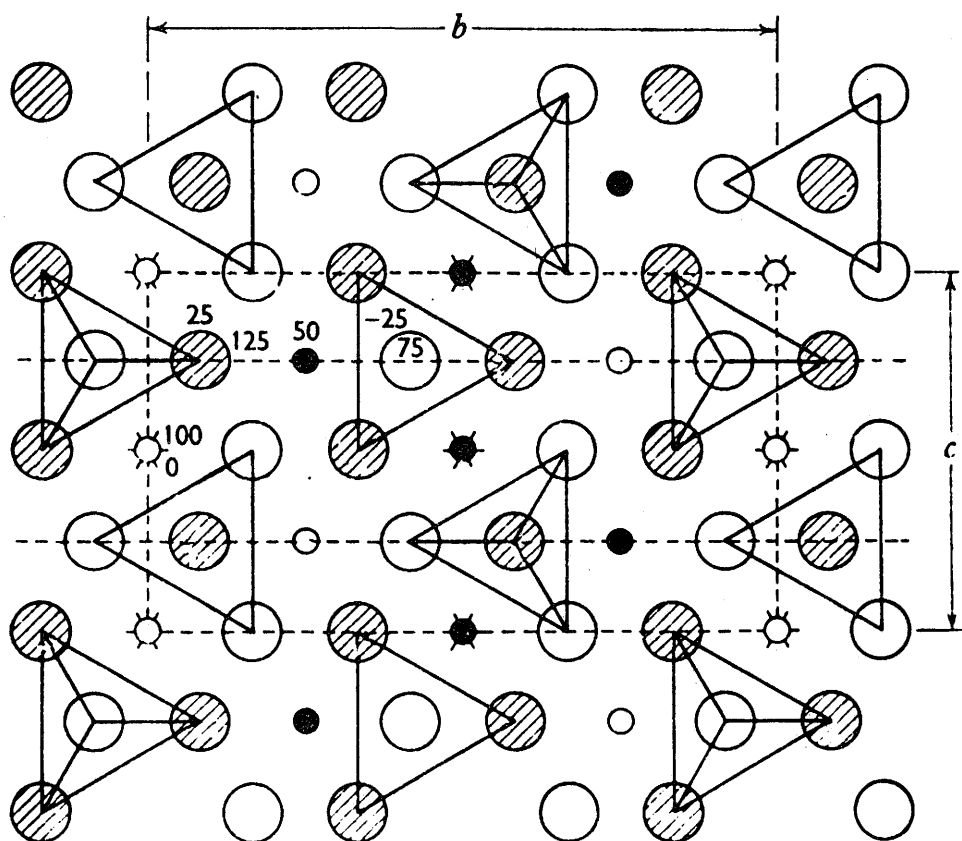


Figure II-5 Olivine structure parallel to (100) plane. Si atoms which are at the centers of the tetrahedra, are not shown. Small open circles \circ Mg atoms at $x = 0$; small solid circles \bullet Mg atoms at $x = \frac{1}{2}$. After Bragg and Brown⁽⁴⁸⁾.

of the three polymorphs of enstatite are shown in Figure II-6.

II.6 The Defect Structure of Forsterite

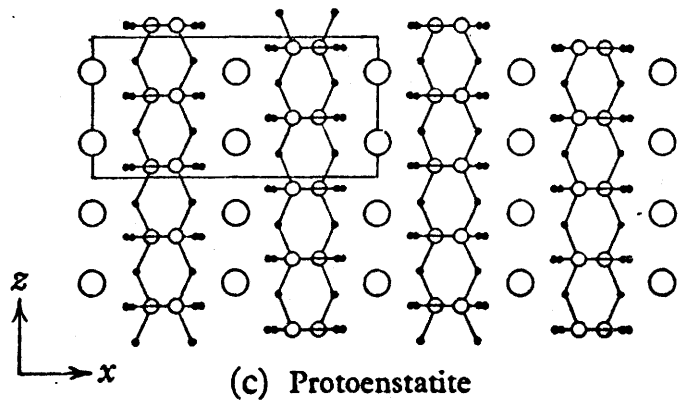
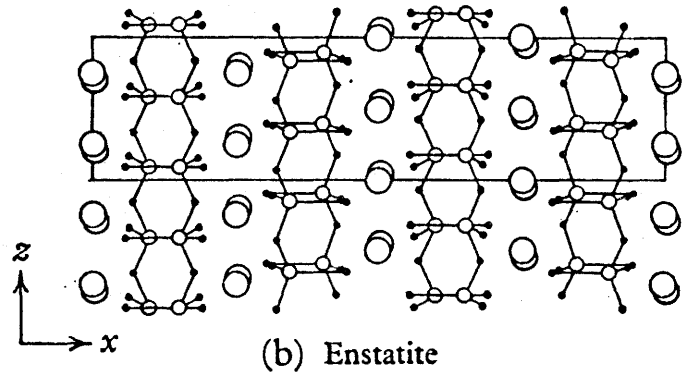
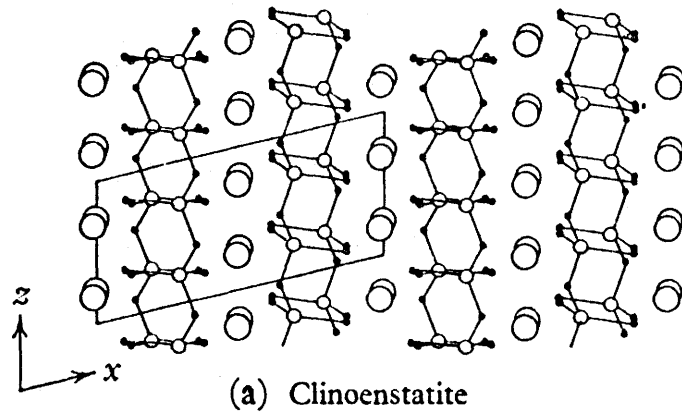
In any system where the reactants must diffuse through a product layer, the defect structure of the product layer will have a profound influence on the rate of reaction, therefore a knowledge of the defect structure is important in understanding the reaction.

According to Borchardt & Schmalzried⁽¹⁷⁾, it is possible to make the following assumptions in deriving the defect structure of forsterite.

- a) Oxygens in interstitial sites are not possible due to the packing density of the oxygen lattice.
- b) The occurrence of cations on anion sites, and vice versa is not possible on the grounds of electrostatic repulsions.

By combining the effective negative and effective positive point defects, it is then possible to form eighteen defect structures, as shown in Table II-1. Defect structures involving silicon ions in octahedral sites and magnesium ions in tetrahedral sites are further discounted for energetic reasons. Further, it is very unlikely that silicon ion vacancies exist because it would require the silicon to be removed from the oxygen lattice. The defects which therefore predominate, according to this scheme, are the Frenkel defect, $(\text{Mg}_{i,0}^{\cdot\cdot}) = (\text{V}_{\text{Mg},0}^{\prime\prime})$, at stoichiometric compositions and the defect types, $(\text{Si}_{i,T}^{\cdot\cdot\cdot}) = \frac{1}{2}(\text{V}_{\text{Mg},0}^{\prime\prime})$ and $(\text{V}_O^{\prime\prime}) = (\text{V}_{\text{Mg},0}^{\prime\prime})$, which predominate when there is a slight excess of SiO_2 . Conductivity measurements on Mg_2SiO_4 with and without excess SiO_2 have confirmed that these are the predominate defect species^(18,19).

According to the Gibbs phase rule, forsterite, being a ternary ionic solid, will require four independent thermodynamic variables to be



○ Mg ○ Si • O

Figure II-6 The structure of a) clino - enstatite, b) enstatite, and c) proto - enstatite projected on the (010) plane. The unit cells of each structure are outlined. After Morimoto⁽⁴⁹⁾.

Table II-1 The Ionized Point Defects in Forsterite
and the Probable Defect Types.
From Borchart and Schmalzried⁽¹⁷⁾.

	$Mg_{Si,T}^{''}$	$V_{Si,T}^{''''}$	$V_{Mg,O}^{''}$
$Si_{i,O}^{''}$			
$Si_{Mg,O}^{''}$			
$Mg_{i,T}^{''}$			
$Si_{i,T}^{''}$			+
$Mg_{i,O}^{''}$			±
$V_{\ddot{O}}$			+

- V \equiv vacancy
 i,O \equiv interstitial site with octahedral coordination
 i,T \equiv interstitial site with tetrahedral coordination
 O \equiv oxygen
 Si,T \equiv regular silicon site with tetrahedral coordination
 Mg,O \equiv regular magnesium site with octahedral coordination
 $+$ \equiv SiO_2 excess
 \pm \equiv stoichiometric compound

The diagonal lines indicate point defects which are not considered to exist.

fixed in order to completely define its thermodynamic state. The choice of pressure and temperature are obvious, and oxygen partial pressure can be readily controlled. The fourth variable requires more attention in choosing for it must be a measure of the stoichiometry of the forsterite. This is perhaps most readily achieved by fixing the activity of SiO_2 in the system.

The variation of the defect structure of the forsterite with a_{SiO_2} can be analyzed by the method of Schmalzried⁽²⁰⁾. By combining the mass and site balance equations, of the form, $\text{SiO}_2 + 2\text{Mg} \rightleftharpoons \text{Si}_i + 2\text{MgO}$, and other similar equations with the integrated form of the Gibbs - Duhem relationship $a_{\text{MgO}}^2 a_{\text{SiO}_2} = \exp \Delta G^\circ / RT$ (ΔG° = free energy of the reaction $2\text{MgO} + \text{SiO}_2 \rightleftharpoons \text{Mg}_2\text{SiO}_4$), it is possible to obtain a general equation for the variation of the log defect concentration with $\log a_{\text{SiO}_2}$.

$$d \log(i) = n_i d \log a_{\text{SiO}_2} \quad (1)$$

where i = a defect

n_i = characteristic number for each defect type.

Graphical representation of these equations, for each defect type, can be made with a Kröger-Vink diagram. The Kröger-Vink diagram for forsterite is shown in Figure II-7. In these diagrams, it is assumed that one disorder type predominates in a particular range of $\log a_{\text{SiO}_2}$. Changing $\log a_{\text{SiO}_2}$ may cause other disorder types to predominate, but it is always assumed that in each region there is always only one major type of disorder. These diagrams have been drawn without regard for the possible formation of new phases. A new phase will form when $\log a_{\text{SiO}_2} = 0$ or when $\log a_{\text{SiO}_2} = \Delta G^\circ / RT - \log a_{\text{MgO}}^2$ (a° = activity of MgO at MgSiO_3 - Mg_2SiO_4 boundary) in which case forsterite will coexist with SiO_2 or MgSiO_3 respectively. A detailed description on how Kröger-Vink calculated these diagrams is given in Appendix I.

The characteristic defect coefficient, n_i , can be related to

KROGER-VINK DIAGRAM FOR Mg_2SiO_4

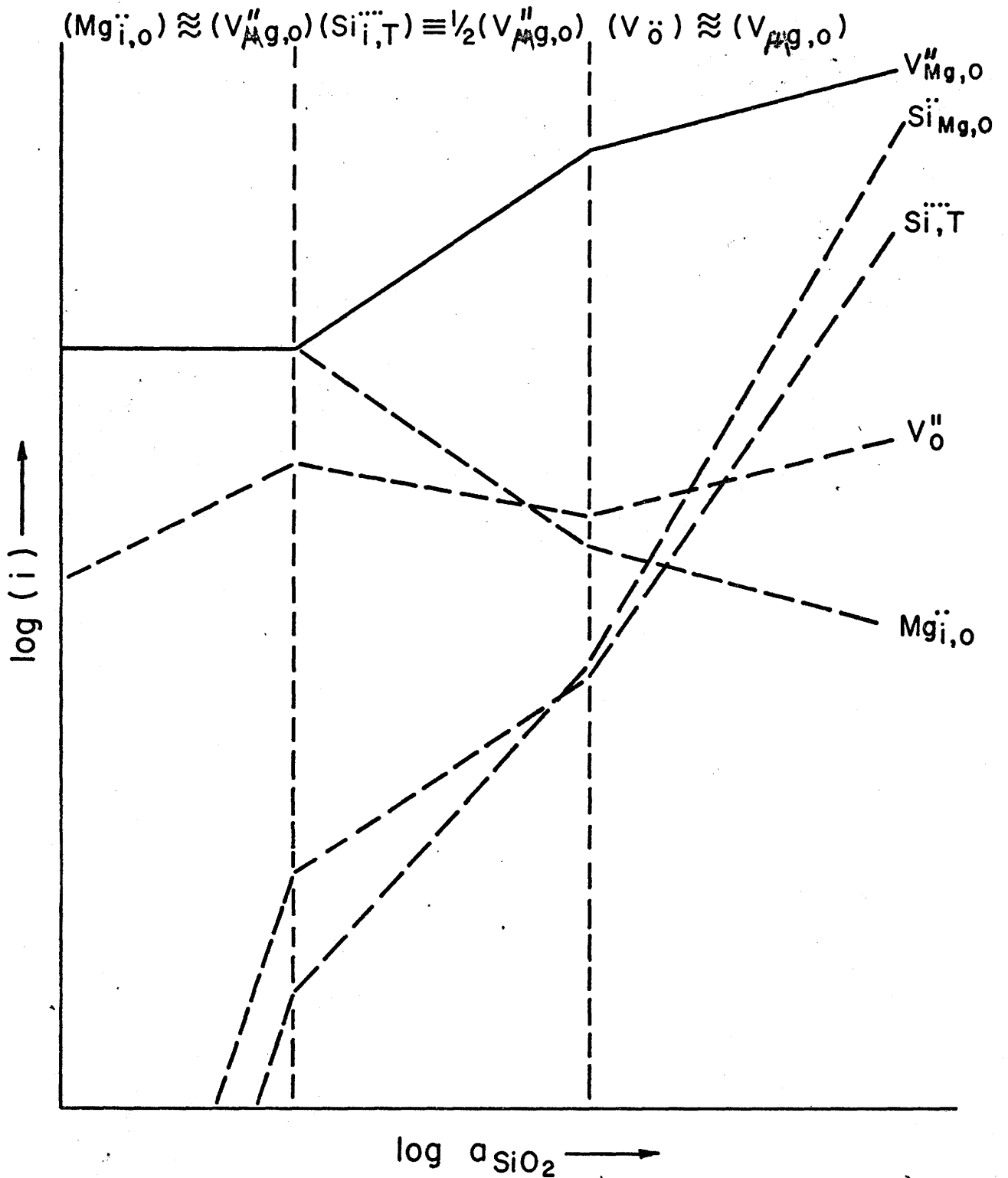


Figure II-7 Kröger - Vink diagram for Mg_2SiO_4 .

measurable properties such as self - diffusion, ionic conductivity, and parabolic rate constants. Schmalzried⁽²⁰⁾ has shown for example that the ratio in self - diffusion coefficients of a silicate in equilibrium with an oxide, AO, and a silicate in equilibrium with SiO₂ may be written in the form

$$\frac{D_i(a_{AO} = 1)}{D_i(a_{SiO_2} = 1)} = \exp n_i \frac{\Delta G^\circ}{RT} \quad (2)$$

where i = any ion or vacancy

II.7 Review of Previous Work on the Reaction Between MgO-SiO₂

II.7-1 Reaction Kinetics in the System MgO-SiO₂

The reaction between MgO and SiO₂ was initially studied by Jander and Wuhrer⁽⁴⁾ in the temperature range 1100°C - 1300°C and by Degueldre⁽⁵⁾ in the temperature range 700°C - 1200°C. Both investigators used fine mixed powders of MgO and SiO₂ and the formation of the product was determined by quantitative X-ray diffraction. Degueldre found that enstatite is the major product formed below 800°C, whereas at 1200°C the major product was forsterite with only trace amounts of enstatite. He also showed that a partial pressure of water vapour dramatically increases the rate of formation of forsterite.

Brindley & Hayami⁽⁶⁾ studied the formation of forsterite using carefully sized powders of MgO and SiO₂ in the temperature range 1100 - 1400 °C. The development of forsterite was again followed by quantitative X-ray diffraction. The results were analysed using the Ginstling - Brounshtein equation^(21,22). In this model it is assumed that the reaction is diffusion controlled. The fraction of material reacted, α , is related to the reaction time by the equation,

$$D(\alpha) = (1 - 2/3\alpha) - (1 - \alpha)^{2/3} = (K/R^2)t \quad (3)$$

where K is the reaction constant and R is the particle radius. Plots of $D(\alpha)$ versus t were used to give a straight line from which K was found. By using a reduced time scale, data for all temperatures can be plotted on a single curve and compared with a theoretical equation. This is done by selecting a particular time, $t_{0.6}$, for each temperature where $\alpha = 60\%$. Then from equation 3;

$$D(0.6) = 0.0571 = (K/R^2)t_{0.6} \quad (4)$$

Combining equations 3 and 4 gives,

$$D(\alpha) = 0.0571(t/t_{0.6})$$

(5)

Figures II-8 and II-9 show plots of α versus the reduced time scale $t/t_{0.6}$ for the results of Brindley & Hayami. The reasonable agreement with equation 5 shows that the reaction is diffusion controlled. The activation energy was found to range from 70 - 80 kcal/mole, depending on the initial size of the reactent powders. They were also able to show by marker experiments that MgO diffused into silica to form Mg_2SiO_4 .

Hayami and Ogura⁽⁷⁾ followed up this work by examining the rate of formation of forsterite from $MgSiO_3$ and MgO. They also re-examined the formation of forsterite from MgO and SiO_2 in the temperature range 1100 °C to 1350 °C. Again sized powders were utilized in conjunction with quantitative X-ray diffraction. Their results were also analysed using the Ginstling - Brounshtein equation. This study showed that the rate of formation of forsterite from enstatite - MgO compacts was approximately ten times greater than the rate from SiO_2 - MgO compacts at all temperatures studied. The activation energies for the reaction $MgSiO_3 + MgO \rightarrow Mg_2SiO_4$ were found to be between 106 and 110 kcal/mole. For the reaction $2MgO + SiO_2 \rightarrow Mg_2SiO_4$, the activation energy was found to be 92 to 110 kcal/mole depending on whether the reaction was followed by the formation of forsterite or the disappearance of cristobalite. Marker experiments carried out on enstatite - MgO couples showed that Mg^{2+} and O^{2-} were the diffusing species. On the basis of these experiments, Hayami and Ogura concluded, " the rate controlling process for the MgO - SiO_2 reaction arises from the diffusion of Mg through the thin enstatite layer which forms between the main reaction product (forsterite) and the SiO_2 component. "

More recent work by Daemgen⁽²³⁾ claims that clino-enstatite is the main reaction product in MgO - SiO_2 couples studied in the temperature

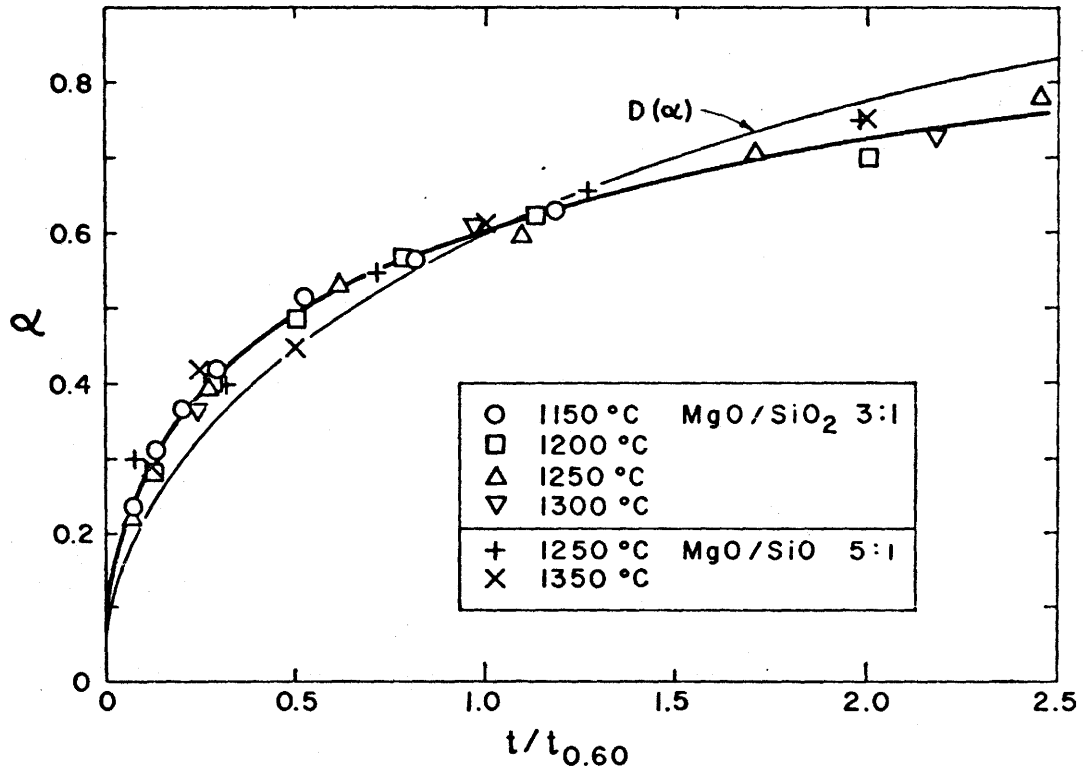


Figure II-8 Formation of forsterite expressed as a percentage, α , of the maximum amount which can be formed by 3 : 1 and 5 : 1 MgO - SiO₂ mixtures, as a function of $t/t_{0.60}$, for various reaction temperatures. Reacting powders; 13 μ cristobalite particles in fine-grained MgO matrix. Heavy line, mean experimental curve; light line, theoretical. From Brindley - Hayami⁽⁶⁾.

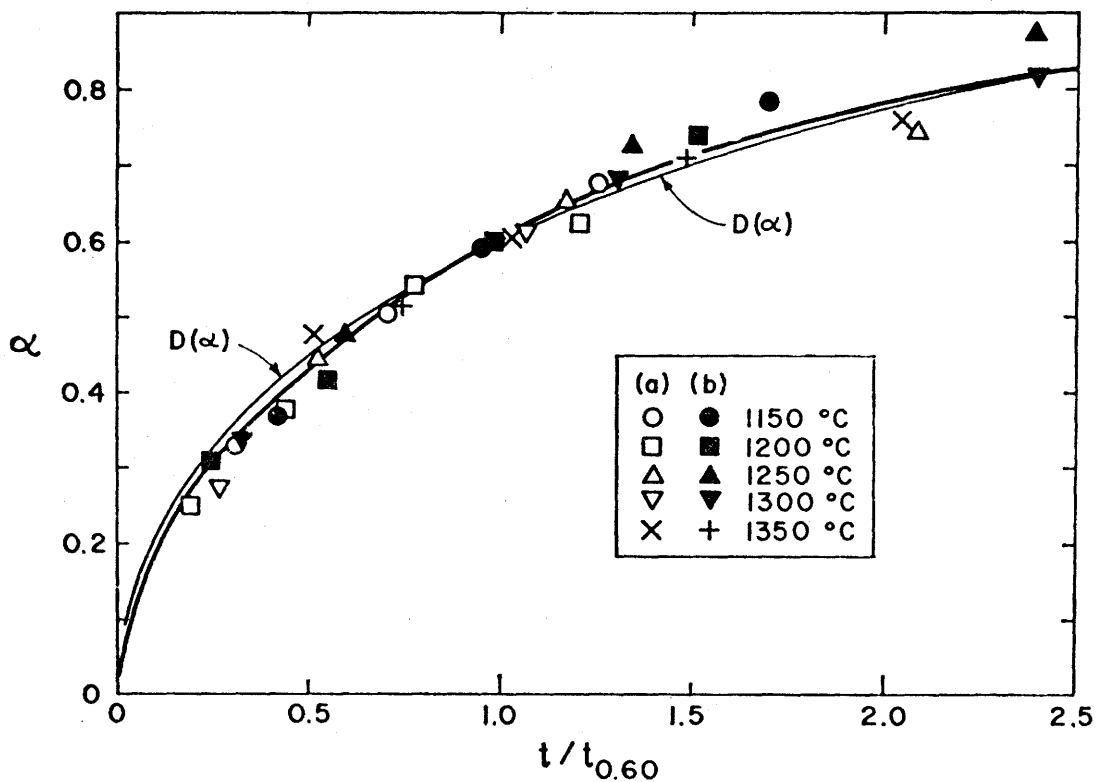


Figure II-9 Formation of forsterite by 14μ MgO particles in a matrix of micron sized quartz powder, (a) based on direct measurement of forsterite formed, (b) indirect measurement based on diminution of amount of MgO. Heavy line, mean experimental curve; light line, theoretical curve. From Brindley and Hayami⁽⁶⁾.

range 1400 ° - 1500 ° C. Couples made of single crystal MgO surrounded by SiO₂ powder were reacted at temperature for periods up to 788 hours, and it was found that only minor amounts of forsterite formed compared with the amount of enstatite formed. Efforts to establish which kinetic law the system followed were unsuccessful, however it was shown that changing the oxygen partial pressure from 1 to 10⁻¹² atm caused no noticeable change in reaction rate, indicating that a mechanism involving the gas phase transport of oxygen is unlikely. The work by Daemgen appears to conflict with previous studies which found forsterite to be the major product with only trace amounts of enstatite. No explanation is advanced for this discrepancy.

The acceleration of the formation of forsterite in the presence of a partial pressure of water vapor was noted by Jander and Wuhrer⁽⁴⁾ and by Degueldre⁽⁵⁾. Osborn⁽²⁴⁾ also noted that very fine ground quartz and MgO yield forsterite at 500° - 700° C under a water pressure of 22.5 - 84 kg/cm² in only 2 - 3 hours. Under these conditions the synthesis of forsterite in a dry system is practically impossible.

The enhancing effect of water in the formation of ortho-silicates has been noted in other systems. In the CaO - SiO₂ system, for example, Burte and Nicholson⁽²⁵⁾ noticed that the rate of formation of CaSiO₄ from CaO and β-quartz was significantly higher in wet than in dry atmospheres.

II.7-2 Thermodynamic Data for the System MgO - SiO₂

Free energy of formation values for the magnesium silicates are not consistent within the literature. For the reaction $\text{MgO} + \text{MgSiO}_3 \rightarrow \text{Mg}_2\text{SiO}_4$, reported values range between $\Delta G^\circ = -7.3$ kcal/mole at 1400 °C⁽²⁶⁾ to $\Delta G^\circ \leq -4.5$ kcal/mole at 1400 °C⁽²⁷⁾ and $\Delta G^\circ = -4.3$ kcal/mole at 1550 °C⁽²⁸⁾.

Rog et al⁽²⁹⁾ determined the free energies of formation of enstatite

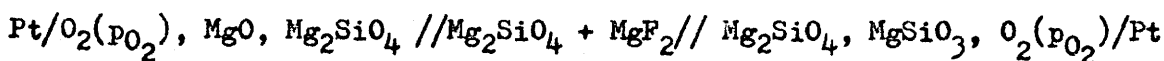
and forsterite from MgO and SiO_2 between 1100° and 1400° C. The electromotive forces of the reactions



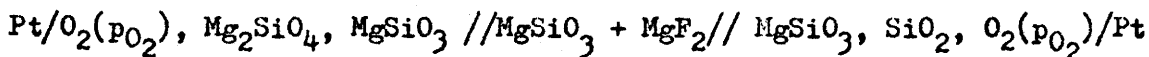
and



were investigated using the solid state galvanic cells



for reaction I, and



for reaction II. Because of the low melting point of MgF_2 (1266° C), it was necessary to use Mg_2SiO_4 as a skeleton to support MgF_2 in the first cell, and $MgSiO_3$ as a skeleton support in the second cell. The ΔG° values for reactions I and II were calculated according to the equation

$$\Delta G^\circ = -z \cdot E \cdot F \quad (6)$$

where z = valence of transport ion (Mg^{2+} , $z = 2$)

E = EMF of cell

F = Faraday's constant

EMF measurements made on heating and cooling cycles did not show any differences. Their findings can be summarized thus:

For reaction I

$$\Delta G^\circ_I = -4,800(\pm 100) - 1.6(\pm 0.1)T \text{ cal/mole} \quad (7)$$

For reaction II

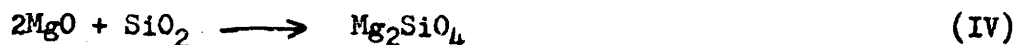
$$\Delta G^\circ_{II} = -4,360(\pm 30) + 2.14(\pm 0.02)T \text{ cal/mole} \quad (8)$$

The free energies of formation of enstatite and forsterite are found by

combining ΔG°_I and ΔG°_{II} , i.e. for the reactions



$$\Delta G^\circ_{\text{III}} = \Delta G^\circ_I + \Delta G^\circ_{\text{II}} = -9,160(\pm 100) + 0.54(\pm 0.1)T \text{ cal/mole} \quad (9)$$

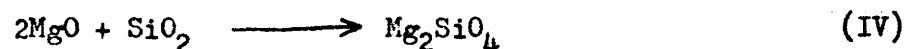
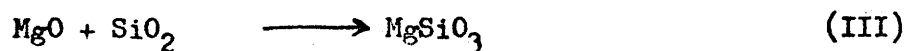
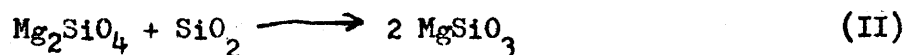
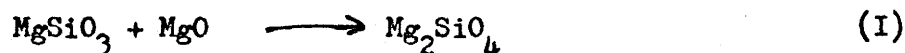


$$\Delta G^\circ_{\text{IV}} = 2\Delta G^\circ_I + \Delta G^\circ_{\text{II}} = -13,960(\pm 100) - 1.06(\pm 0.1)T \text{ cal/mole} \quad (10)$$

According to the data of Rog et al, the free energy of formation of enstatite and forsterite from MgO and SiO_2 at 1400 °C would be -8.26 ± 0.26 kcal/mole and -15.73 ± 0.26 kcal/mole respectively.

II.8 Review of Solid State Reaction Kinetics

In the $\text{MgO} - \text{SiO}_2$ system, there are four possible reactions namely;



Forsterite may form in a one step reaction as in IV, or in two discrete reactions as described in I and III. Reactions II and III describe the possible reactions for the formation of enstatite.

The above reactions may be studied by placing two reactant oxides along a planar interface. As the reaction proceeds, a layer of product oxide will grow between the two starting oxides. According to Wagner⁽³⁰⁾ the growth of the product will be parabolic if the following conditions hold:

1) the reaction layer is dense, and does not contain nonequilibrium defects such as dislocations and grain boundaries.

2) interface reactions are fast in comparison with the transport of the reactants across the product layer.

3) diffusing species are coupled only by requirements of local equilibrium and electroneutrality, and otherwise move independently.

4) thermodynamic equilibrium exists at phase boundaries.

If these conditions are met, the product layer growth will be inversely proportional to its thickness.

$$\frac{dx}{dt} = \frac{k_p}{x} \quad (11)$$

where x = product layer thickness

k_p = parabolic rate constant

t = time

On integration, the well known parabolic rate law will be derived

$$x^2 = 2k_p t - x_0^2 \quad (12)$$

where x_0^2 = constant of integration

Marker experiments can aid in the determination of the mechanism in a diffusion controlled reaction. For reaction IV, there are eight possible mechanisms as listed in Table II-2. These mechanisms are divided into three groups according to the rate controlling diffusing species.

Mechanisms I and IV represent inverse cation diffusion through the silicate layer. The reaction proceeds by,

a) dissociation of MgO into Mg^{2+} and O^{2-} , and of SiO_2 into Si^{4+} and $2O^{2-}$.

b) countercurrent diffusion of Mg^{2+} and Si^{4+} leaving the O^{2-} behind in the starting oxides.

c) reaction of Si^{4+} , $2MgO$, and $2O^{2-}$ to form Mg_2SiO_4 at the $MgO - Mg_2SiO_4$ interface, and the reaction of $2Mg^{2+}$ with SiO_2 and $2O^{2-}$ to

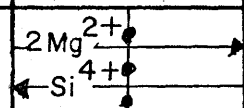
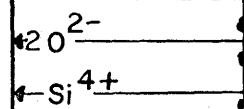
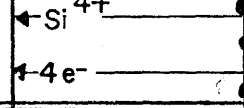
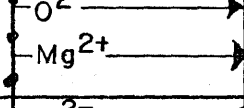
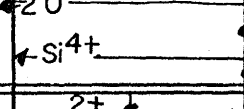
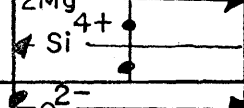
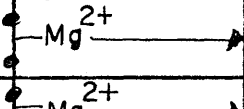
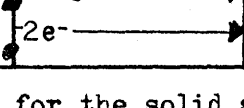
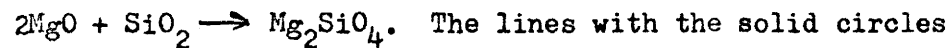
Diffusivities		γ	MgO Reaction at the MgO-Mg ₂ SiO ₄ interface	Mg ₂ SiO ₄ Ion transport	SiO ₂ Reaction at the SiO ₂ -Mg ₂ SiO ₄ interface
I	$D_{Mg} \gg D_{Si} \gg D_O$	4	$Si^{4+} + 4MgO = Mg_2SiO_4 + 2Mg^{2+}$		$2Mg^{2+} + 2SiO_2 = Mg_2SiO_4 + Si^{4+}$
II	$D_O \gg D_{Si} \gg D_{Mg}$	1	$2MgO + Si^{4+} = Mg_2SiO_4$		$SiO_2 = Si^{4+} + 2O^{2-}$
III	"	1	$Si^{4+} + 4e^- + O_2(g) + 2MgO = Mg_2SiO_4$		$SiO_2 = Si^{4+} + 4e^- + O_2(g)$
IV	$D_{Mg} \gg D_O \gg D_{Si}$	1	$MgO = Mg^{2+} + O^{2-}$		$Mg^{2+} + O^{2-} + 1/2SiO_2 = 1/2Mg_2SiO_4$
V	$D_{Si} \gg D_O \gg D_{Mg}$	1	$2MgO + Si^{4+} + 2O^{2-} = Mg_2SiO_4$		$SiO_2 = Si^{4+} + 2O^{2-}$
VI	$D_{Si} \gg D_{Mg} \gg D_O$	2	$Si^{4+} + 4MgO = Mg_2SiO_4 + 2Mg^{2+}$		$2Mg^{2+} + 2SiO_2 = Mg_2SiO_4 + Si^{4+}$
VII	$D_O \gg D_{Mg} \gg D_{Si}$	1/2	$MgO = Mg^{2+} + O^{2-}$		$Mg^{2+} + O^{2-} + 1/2SiO_2 = 1/2Mg_2SiO_4$
VIII	"	1/2	$MgO = Mg^{2+} + 2e^- + 1/2O_2(g)$		$Mg^{2+} + 2e^- + 1/2O_2(g) + 1/2SiO_2 = 1/2Mg_2SiO_4$

Table II-2 The possible reaction mechanisms for the solid state reaction



The lines with the solid circles indicate the original interface, and the arrows show the direction of ion transport.

form Mg_2SiO_4 at the $\text{SiO}_2 - \text{Mg}_2\text{SiO}_4$ interface.

In order to maintain electroneutrality across the product layer, 2Mg^{2+} ions must diffuse for every one Si^{4+} ion. This results in one Mg_2SiO_4 unit forming at the $\text{MgO} - \text{Mg}_2\text{SiO}_4$ interface for every Mg_2SiO_4 formed at the $\text{SiO}_2 - \text{Mg}_2\text{SiO}_4$ interface, causing the original reactant oxide interface to be located in the exact middle of the product phase.

Mechanisms II and V are due to diffusion of Si^{4+} and O^{2-} through the product layer. The sequence of this reaction will be,

- a) dissolution of SiO_2 into Si^{4+} and 2O^{2-} .
- b) diffusion of Si^{4+} and 2O^{2-} through the product layer.
- c) reaction of Si^{4+} and 2O^{2-} with 2MgO to form Mg_2SiO_4 at the $\text{MgO} - \text{Mg}_2\text{SiO}_4$ interface.

In this case the $\text{SiO}_2 - \text{Mg}_2\text{SiO}_4$ interface will correspond to the original reactant oxide interface.

Mechanisms IV and VII are similar to II and V, but in this case the product forms due to diffusion of Mg^{2+} and O^{2-} . The sequence in this mechanism

- a) dissociation of MgO into Mg^{2+} and O^{2-} .
- b) transport of 2Mg^{2+} and 2O^{2-} across the product layer.
- c) the reaction of 2Mg^{2+} and 2O^{2-} with SiO_2 to form Mg_2SiO_4 .

The original reactant oxide interface will now be the $\text{MgO} - \text{Mg}_2\text{SiO}_4$ interface.

Mechanisms III and VIII involve the transport of oxygen through the gas phase, and of electrons through the product layer. This mechanism was put forward because it allows an alternate means of oxygen transport other than oxygen anion diffusion, which in many ceramic systems is extremely slow. This mechanism can only operate when there is a sufficient oxygen partial pressure, and when there is no restriction to transport in the gas

phase. The product layer must also be an electronic conductor. Markhasev⁽³¹⁾ has suggested that a gas phase transport of oxygen mechanism may occur in the MgO - SiO₂ and other ceramic systems. The sequence of this mechanism is as follows,

- a) dissociation of MgO into Mg²⁺ and O²⁻.
- b) reaction of O²⁻ to form O₂ gas and two electrons.
- c) simultaneous transport of O₂ through the gas phase and Mg²⁺ and electrons through the product layer.

- d) the reaction of 2 Mg²⁺, O₂, and 4e⁻ with SiO₂ to form Mg₂SiO₄.

Wagner⁽³⁰⁾ and Schmalzried^(32,33) have attempted to derive a theoretical relationship between the parabolic rate constant, the mechanism, diffusion coefficients, and the free energy of formation of a silicate. The theory was originally derived for the solid state formation of spinels, however the theory may readily be applied to silicate formation. The following derivation is adapted from one given by Armigo in a review article on spinel formation⁽³⁴⁾.

The derivation for the case $D_{Mg} \gg D_O \gg D_{Si}$ will be considered. The derivations for the other mechanisms are similar. If the magnesium cation is the fastest diffusing species then the oxygen anion will be the rate controlling diffusing species, and silicon will diffuse so slowly as to take no part in the reaction. The flux in equivalents of the individual ions is given by

$$j_i = \frac{D_i c_i z_i}{RT} \cdot \frac{d\bar{u}_i}{dx} \quad (13)$$

where D_i = self diffusion coefficient of i

c_i = equivalent concentration of i

z_i = absolute charge of i

$\frac{d\tilde{\mu}_i}{dx}$ = electrochemical potential gradient per equivalent of i
across the reaction layer.

For the mechanism $D_{Mg^{2+}} \gg D_{O^{2-}} \gg D_{Si^{4+}}$

$$j_{Mg} = j_O = j \quad (14)$$

Note: For the sake of clarity the valence numbers of the ions from here on shall be omitted.

Applying the electroneutrality condition

$$j = \left[\frac{(D_{Mg} c_{Mg} z_{Mg}) \cdot (D_O c_O z_O)}{(D_{Mg} c_{Mg} z_{Mg}) + (D_O c_O z_O)} \right] \frac{1}{RT} \left(\frac{d\tilde{\mu}_{Mg}}{dx} + \frac{d\tilde{\mu}_O}{dx} \right) \quad (15)$$

Since $D_{Mg} \gg D_O$

$$j = \left[\frac{D_O c_O z_O}{RT} \right] \left(\frac{d\tilde{\mu}_{Mg}}{dx} + \frac{d\tilde{\mu}_O}{dx} \right) \quad (16)$$

The quantities in the brackets represent average values of the diffusion coefficient and equivalent concentration.

The sum of the electrochemical potentials of the individual ions may be written as the chemical potential of the starting oxides.

$$\text{i.e., } \tilde{\mu}_{MgO} = \tilde{\mu}_{Mg} + \tilde{\mu}_O \quad (17)$$

$$\tilde{\mu}_{SiO_2} = \tilde{\mu}_{Si} + 2\tilde{\mu}_O \quad (18)$$

Substituting $\frac{d\tilde{\mu}_{Mg}}{dx} + \frac{d\tilde{\mu}_O}{dx} = \frac{d\tilde{\mu}_{MgO}}{dx}$ into equation 16 we get

$$j = \left[\frac{D_O c_O z_O}{RT} \right] \left(\frac{d\tilde{\mu}_{MgO}}{dx} \right) \quad (19)$$

where $\frac{d\tilde{\mu}_{MgO}}{dx}$ will be the chemical potential gradient per equivalent of MgO.

The equivalent flux, \dot{n} , across the reaction layer of cross section area, q , per unit time is found by integration of equation 19.

$$\dot{n} = jq \int_0^{x_0} dx = q \left[\frac{D_0 c_0 z_0}{RT} \right] \int_{\tilde{\mu}_{MgO} \text{ at } x=0}^{\tilde{\mu}_{MgO} \text{ at } x=x_0} d\tilde{\mu}_{MgO} \quad (20)$$

$$\dot{n} = \frac{q}{x} \left[\frac{D_0 c_0 z_0}{RT} \right] (\tilde{\mu}_{MgO}'' - \tilde{\mu}_{MgO}') \quad (21)$$

The growth rate of the silicate layer may be given by

$$q \frac{dx}{dt} = V \dot{n} \quad (22)$$

where V = volume of silicate formed per equivalent transported across the product layer.

By combining equations 21 and 22 we have

$$\frac{dx}{dt} = \frac{V}{x} \left[\frac{D_0 c_0 z_0}{RT} \right] (\tilde{\mu}_{MgO}'' - \tilde{\mu}_{MgO}') \quad (23)$$

Comparing the expression with the differentiated form of the parabolic rate law

$$\frac{dx}{dt} = \frac{k_p}{x} \quad (11)$$

it is evident that the parabolic constant, k_p , is equal to

$$k_p = V \left[\frac{D_0 c_0 z_0}{RT} \right] (\tilde{\mu}_{MgO}'' - \tilde{\mu}_{MgO}') \quad (24)$$

Now $V \times c_0 = 1$ and $z_0 = -2$. Because two equivalents of Mg_2SiO_4 are formed when one equivalent of MgO diffuses through the product layer

$$\tilde{\mu}_{MgO}'' - \tilde{\mu}_{MgO}' = \frac{1}{2} \Delta G^\circ_{Mg_2SiO_4} \quad (25)$$

Expression 24 may then be reduced to

$$k_p = -\gamma \bar{D}_0 \frac{\Delta G^\circ}{RT} \quad (26)$$

where $\gamma = 1$ for this mechanism.

Similar relationships can be derived for the other mechanisms. The values of γ for the other mechanisms are given in Table II - 2.

Expression 26 may be developed further. To evaluate the average component diffusion coefficient, D_i , Schmalzried has given the following expression (20)

$$\bar{D}_i = \frac{RT \int_{a'_{MgO}}^{a''_{MgO}} D_i \cdot d \log a_{MgO}}{\mu''_{MgO} - \mu'_{MgO}} \quad (27)$$

From equation 2 we know that;

$$D_i = D_i^\circ \exp n_i \frac{\mu''_{MgO} - \mu'_{MgO}}{RT} \quad (28)$$

Substitution of 28 into 27 yields

$$\bar{D}_i = - \frac{D_i^\circ RT}{n_i \frac{\Delta G^\circ}{2}} \left(1 - \exp \frac{n_i \Delta G^\circ}{2RT} \right) \quad (29)$$

By using this value for \bar{D}_i in the equation for k_p , we get

$$k_p = - \frac{\gamma D_i^\circ 2}{n_i} \left(1 - \exp \frac{n_i \Delta G^\circ}{2RT} \right) \quad (30)$$

D_i° is the self diffusion coefficient of component i in Mg_2SiO_4 which is in equilibrium with MgO . The k_p can, at least in principal, be calculated by knowing the free energy of formation, mechanism, major disorder type, and the self diffusion coefficients. Experimental investigation along

this line has been carried out in a number of spinel systems⁽³⁴⁾, but as of yet such knowledge is not available for the silicate systems.

CHAPTER III

EXPERIMENTAL WORK

III.1 Introduction

In this investigation the reaction between MgO and SiO₂ was studied by embedding a single crystal of quartz in a compact of high purity MgO powder. The thickness of the product layer formed after a period of heating was measured as a function of time. This results in one dimensional growth data on known crystallographic planes of the quartz crystal. Although this method is less convenient than indirect measurements carried out on mixed powders, it eliminates the uncertainties inherent in the mixed powder methods associated with unknown shape factors and particle size distributions.

III.2 Sample Preparation

III.2-1 Starting Materials

The high purity magnesium oxide was obtained by heating high purity electrolytically precipitated Mg(OH)₂* at 1350°C for 24 hours. The purpose of the heating was to dehydrolyse the magnesium hydroxide, and to increase the particle size of the MgO in order to prevent excessive shrinkage due to sintering of the MgO - SiO₂ reaction pellet. The calcined MgO was ground to a uniform powder.

Analysis for CaO and Fe₂O₃ in MgO showed;

* Supplied by Northern Pigment, Toronto Ontario

<u>Lot</u>	<u>CaO ppm wt.</u>	<u>Fe₂O₃ ppm wt.</u>
EL-Mg(OH) ₂ -10	37	24
EL-MgO-6	61	43

The silica was used in the form of hydrothermally grown artificial quartz. The quartz was cut using an Isomet slow speed diamond wheel to expose the basal (0001) and the prism ($\bar{1}\bar{1}00$) planes. The dimensions of the cut quartz crystal were 3 mm parallel to the C-axis, 2 mm parallel to the α -axis, by 1.5 mm. The cut crystals were washed in concentrated sulfuric acid for 24 hours, and then in distilled water to remove the mounting resin used in the cutting of the quartz.

III.2-2 Preparation of Reaction Samples

The reaction couples were prepared by pressing approximately 2 gm of MgO with a centrally located quartz crystal in a 12 mm diameter steel die. The procedure was as follows;

- 1) lightly press (1000 lb) approximately 0.75 gm MgO in the die.
- 2) centrally place the quartz crystal in the die, with the basal and prism planes perpendicular to the bottom of the die.
- 3) carefully add an additional 1.25 gm MgO to cover the quartz crystal and press to 6000 lb.

The procedure results in a MgO - SiO₂ reaction couple which is strong enough to withstand handling and the severe heating rates required by the experiment.

III.2-3 Apparatus

Runs at 1200, 1250, and 1300 °C were performed in a Kanthal horizontal tube furnace. The furnace was equipped with a 20 inch heating

element and an on-off controller capable of controlling to ± 3 °C over a period of three days. The reactions were carried out in an impervious mullite tube, 30 inches long with $1\frac{1}{2}$ " ID. One end of the mullite tube was sealed with an air tight, water cooled brass fitting, through which a thermocouple was fitted, and through which dry or wet nitrogen entered the tube. The other end of the mullite tube was fitted with another air-tight, water cooled brass fitting, which allowed the nitrogen to flow out of the furnace, and which could readily be opened and closed to allow access to the hot zone. At 1200°C, the hot zone of the Kanthal furnace was found to be $2\frac{1}{2}$ " long.

A horizontal SiC tube furnace was used for the runs at 1350 and 1400 °C. The heating element consisted of a solid tube of SiC, 20 inches long, $2\frac{1}{4}$ " OD and $1\frac{3}{4}$ " ID. This furnace was equipped with a proportional input controller, capable of controlling ± 2 °C at 1400°C over a period of twelve hours. A mullite working tube with brass end fittings similar to those used on the Kanthal furnace was used on this furnace. At 1400°C, the hot zone was determined to be $1\frac{1}{2}$ inches in length.

The temperature was measured using a Pt-Pt 10% Rh thermocouple and a Rubicon Model 2710 A potentiometer.

Experiments were carried out in dry and wet nitrogen atmospheres, at 1 atmosphere pressure. The nitrogen was Canadian Liquid Air "L" grade. This nitrogen contained 20 ppm oxygen and 80 ppm argon impurities. For experiments in dry atmospheres, the nitrogen was also dried using a type 4A Molecular Sieve. Wet nitrogen was generated by passing the nitrogen through a series of 4 flasks containing distilled water held in a constant temperature bath. The partial pressure of water was controlled by adjusting the temperature of the bath. Care was taken to heat all tubes carrying wet nitrogen above 100 °C to prevent condensation of the water vapor. The nitrogen flow was

approximately 6 l/hr. for dry nitrogen and 30 l/hr. for wet nitrogen.

III.2-4 Experimental Procedure

Experiments were carried out in dry nitrogen atmospheres at 1203°, 1245°, 1292°, 1349°, and 1415° C. Runs using wet nitrogen were carried out at 1200°C using water partial pressures of 45, 135, and 250 mm Hg.

Each run consisted of up to nine samples placed in an alumina boat. The boat was pushed into the hot zone in such a manner that the rate of heating of the pellets was slow up to 700°C, to allow for the α - β transition in quartz, and rapid from 700°C to the predetermined reaction temperature. At regular intervals the entire alumina boat was rapidly withdrawn from the furnace and one reaction sample removed. The boat containing the remainder of the reaction pellets was then re-introduced into the hot zone. The reacted sample was then air-cooled to room temperature. This procedure resulted in samples which contained no significant cracks. The sample heating time from 700°C to the reaction temperature was under 3 minutes. This heating lag was not considered to be significant.

Reacted samples were vacuum impregnated with Struers Epofix Epoxy resin. The epoxy resin was warmed to 50°C before impregnation to increase fluidity, so ensuring complete impregnation. Once the epoxy had hardened the reaction components were firmly set in their original configuration, allowing the pellets to be sectioned and polished without any damage to the reaction interface.

The hardened epoxy mounted specimens were first roughly polished on a silicon carbide belt grinder to expose the quartz crystal. The quartz crystal was exposed in such a manner that both the basal and prism planes of

* Struers Scientific Instruments, Copenhagen Denmark

the quartz were perpendicular to the ground face. The samples were then successively polished on 2, 1, 0, 2/0, 3/0, and 4/0 emery papers, 6 and 1 micron diamond paste, with kerosene as the lubricant, and 0.3 micron alumina powder using distilled water as the lubricant. The samples were then suitable for examination by an optical microscope and by the electron probe. Thin section samples were also prepared using the Struers Discoplan TS followed by polishing on diamond and alumina powders.

III.2-5 Optical Examination

The optical examination was carried out on a Reichert Universal Camera Microscope at approximately 1000X magnification. The thickness of the product layer was determined using a Bausch & Lomb "Filar Micrometer Eyepiece" calibrated using a stage micrometer. Up to one hundred thickness measurements per specimen were made on both the basal and prism planes of the quartz.

III.2-6 Electron Microprobe Measurements

Examination of the regions adjacent to the reaction interface to determine the composition of the product layer was carried out using the Cameca MS-64 electron microprobe. To eliminate the need for atomic number, absorption and fluorescence corrections, standards of forsterite and enstatite as well as single crystal MgO, sintered MgO, and single crystal quartz were used. The preparation of forsterite and enstatite are described in Appendix II. Step counts were taken across the interface of an MgO-quartz couple reacted at 1340°C for 24 hours. The acceleration voltage was set at 16KV with a 125 nano-ampere current. The RAP crystal was used for MgK α radiation, and the mica crystal for the SiK α radiation. The scan was taken across the quartz-product-MgO interface in such a manner that the direction of the

spectrometers was parallel to the interface. Twenty second step counts were taken at 0.5μ intervals. The estimated beam diameter was 3μ and the product layer was about 8μ thick.

III.2-7 X-ray Diffraction

X-ray diffraction experiments were conducted for two reasons

- 1) to determine which products had formed.
- 2) to determine to what extent quartz had transformed to some other form of silica.

The difficulties of obtaining sufficient amounts of product for X-ray analysis when dealing with the product layers of $5-10 \mu$ are apparent. An in-situ method was therefore attempted. This method entailed the careful breaking out of the reacted quartz crystal from the MgO matrix and then carefully mounting it in a Debye-Scherrer camera so that the incident X-ray beam struck the quartz crystal at an angle of 60° to the $(11\bar{2}0)$ axis. The sample was positioned so that the beam passed through the edge of the specimen. See Figure III-1. The patterns so obtained were the single crystal spot pattern of the quartz superimposed on the Debye-Scherrer pattern of the products.

Two sets of samples were examined by this method,

- 1) samples heated at 1340°C for 24 hours, similar to those examined on the electron probe.
- 2) samples heated at 1450°C for 24 hours.

A 11.5 cm diameter Debye-Scherrer camera was used, with Ni filtered $\text{CuK}\alpha$ radiation.

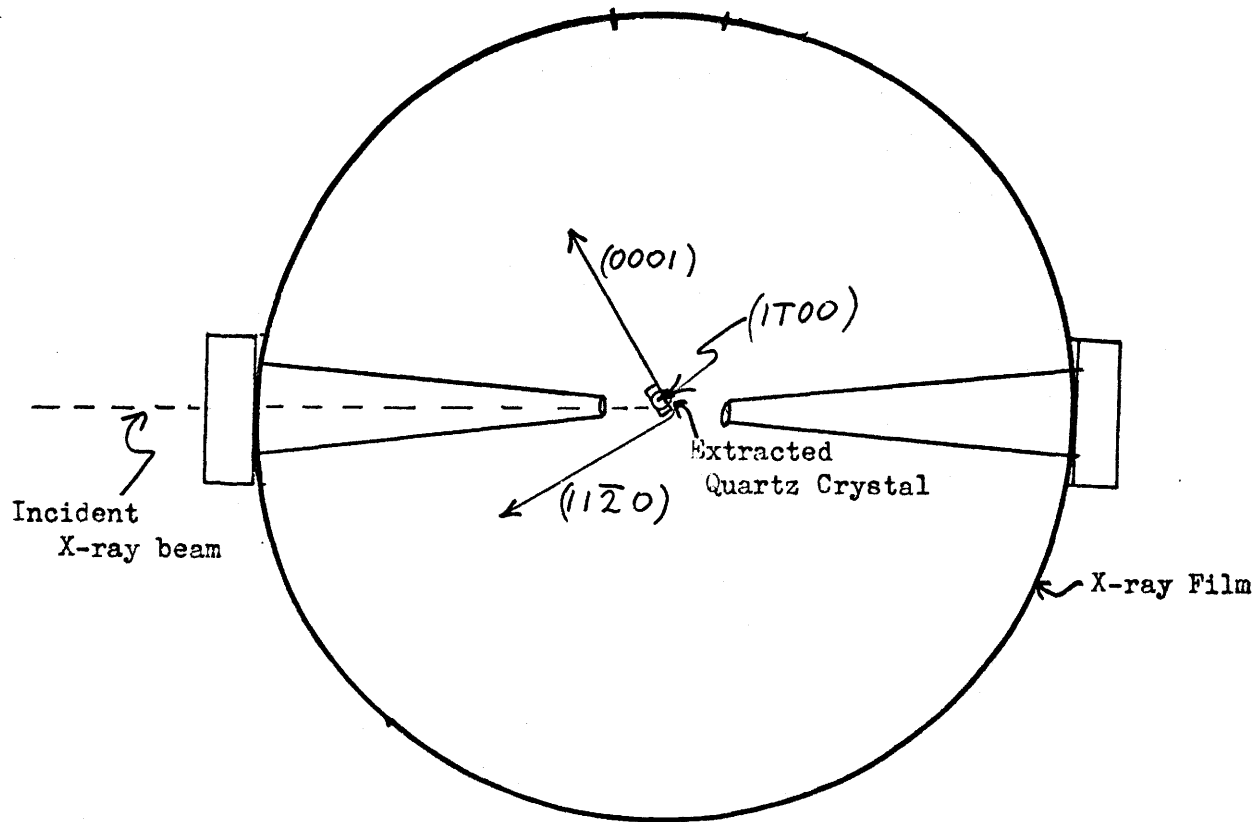


Figure III-1 The position of the reacted quartz pellet in the Debye - Scherrer Camera.

CHAPTER IV

RESULTS AND DISCUSSION

IV.1 Morphology and Composition of Reaction Product

The morphology and kinetics of the reaction between β - quartz and MgO was studied between 1200 °C and 1400 °C. Figure IV - 1 shows the reaction interface on the prism plane of quartz after heating at 1250 °C for 48 hours. The smooth condition of the quartz indicates that its transformation to a more stable polymorph of silica has not occurred. A distinct reaction product layer of uniform thickness is evident between the quartz and MgO. The reaction couple formed at higher temperatures is shown in Figure IV - 2. This couple was heated at 1340 °C for 24 hours and shows that the single crystal quartz has started to fragment. This condition is the initial step in its transformation, however no second phase of silica was detectable visually or by X - rays. The epoxy - filled voids are formed due to the sintering and consequent shrinkage of the MgO around the quartz crystal. Figures IV - 3a and IV - 3b show the same section at a higher magnification. These figures show the reaction layers on the basal and prism planes of quartz respectively. Close examination of the reaction layer indicates no observable differences between their thickness or morphology. The product layer is more irregular at this temperature than that formed at 1250 °C. The crack between the product layer and the MgO results from the shrinkage of the quartz on passing through the β - α transition. The original quartz - MgO interface can be seen and it is evident that the MgO -

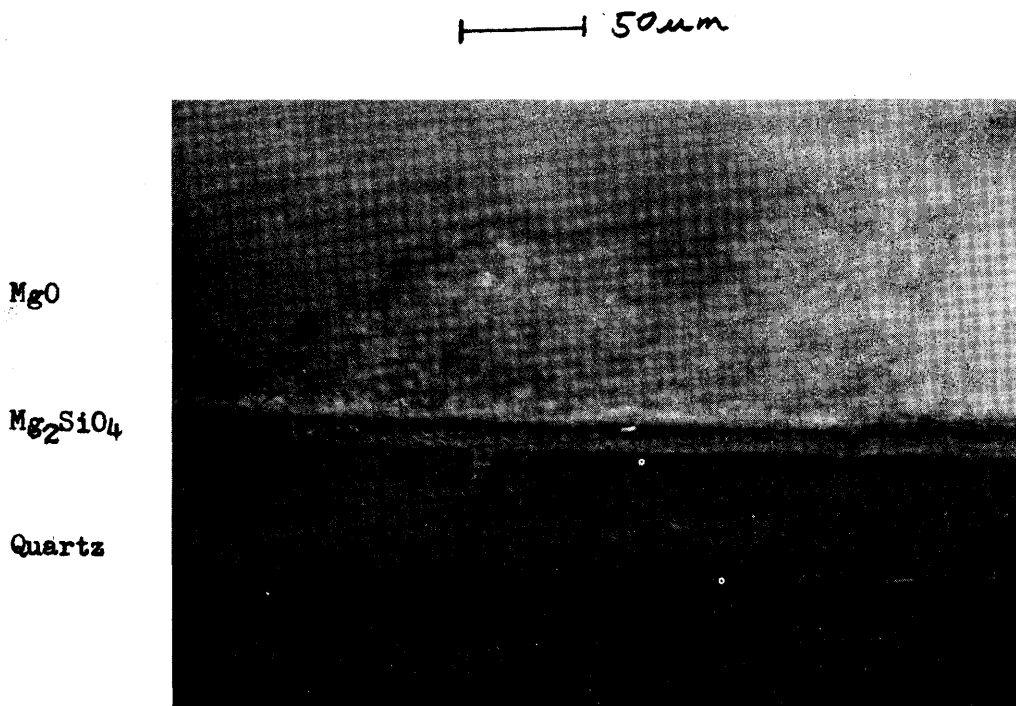


Figure IV-1 The quartz - MgO reaction interface after heating at 1250 °C for 48 hours.

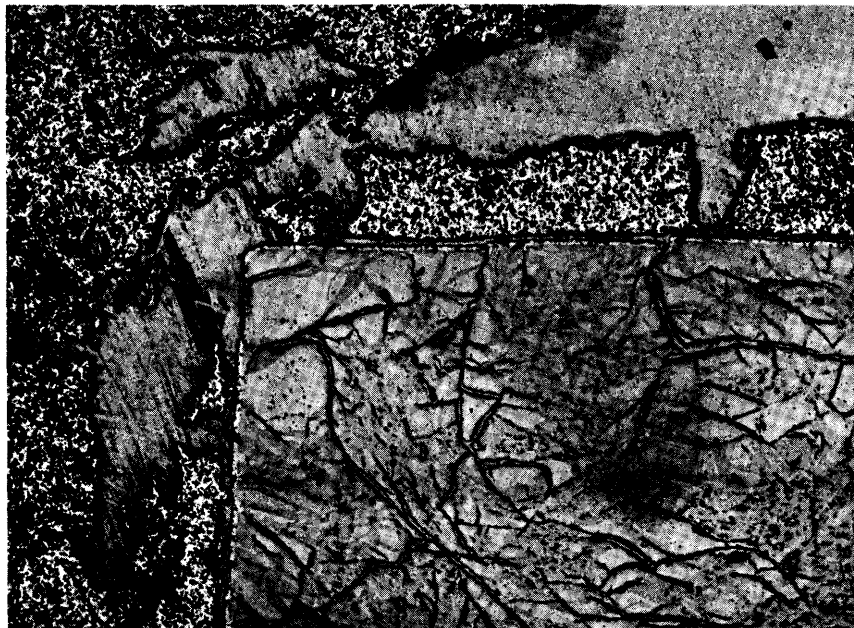


Figure IV-2 A quartz - MgO reaction couple heated at 1340 °C
for 24 hours.

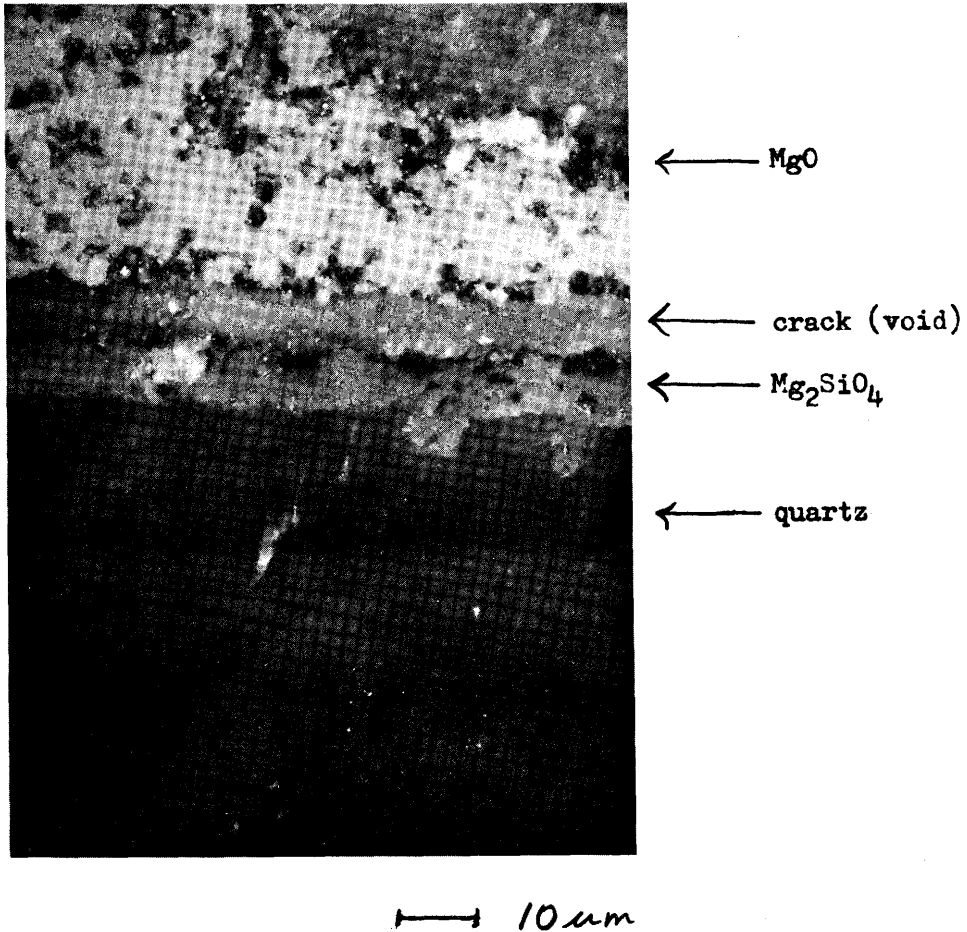
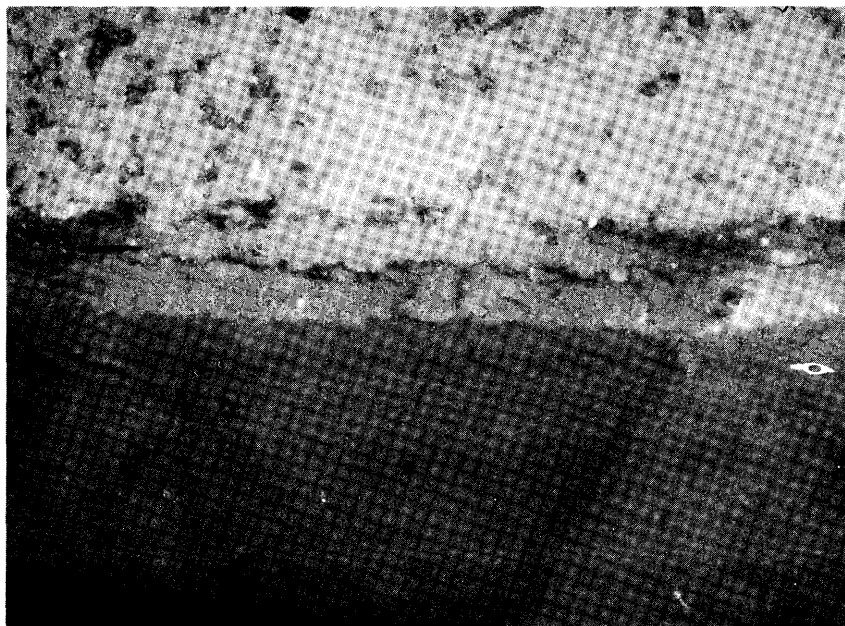


Figure IV-3a The reaction interface on the prism plane of quartz after heating at 1340 °C for 24 hours.



— 10 μm

Figure IV-3b The reaction interface on the basal plane of quartz after heating at 1340 °C for 24 hours.

SiO_2 product layer forms on the quartz side of this interface. This is in agreement with the findings of Degueldre⁽⁵⁾ and the marker experiments of Brindley and Hayami⁽⁶⁾. These results are consistent with a mechanism of Mg^{2+} and O^{2-} diffusion through the product layer, i.e. mechanisms IV, VII, or VIII as listed in Table II - 2. A thin section micrograph of a reaction couple heated at 1340 °C for 24 hours is shown in Figure IV - 4. The colour in the product layer shows that it is crystalline, however no clear extinction angle could be found under crossed nicols. This suggests that the product is in the form of very fine crystallites of random orientation⁽³⁹⁾. The highly strained state of quartz, due to heating above its stability range for extended periods of time is evident in micrograph.

Only one product is detected in both the transmitted and reflected light micrographs. The vacuum impregnated reaction couples were etched using NaOH, HCl, and HF vapour in an attempt to determine if the product layer contained more than one compound. Hydrochloric acid was used as an etchant because it is known that forsterite, Mg_2SiO_4 , will dissolve in HCl, while enstatite, MgSiO_3 , and silica, SiO_2 , are insoluble. The acid - base reaction between HCl and MgO caused rapid dissolution of the MgO phase, making it impossible to interpret the results. Similar problems were found using HF vapour as the etchant. Etching with NaOH did not alter the reaction interface. No conclusive evidence as to whether the product layer consisted of both forsterite and enstatite, or only one of these compounds could be obtained by etching techniques.

The composition of the product layer was determined by electron microprobe analysis. Point counts of the product layer were compared with enstatite and forsterite standards. An interface scan of the couple reacted at 1340 °C for 24 hours is shown in Figure IV - 5. The scan begins on the

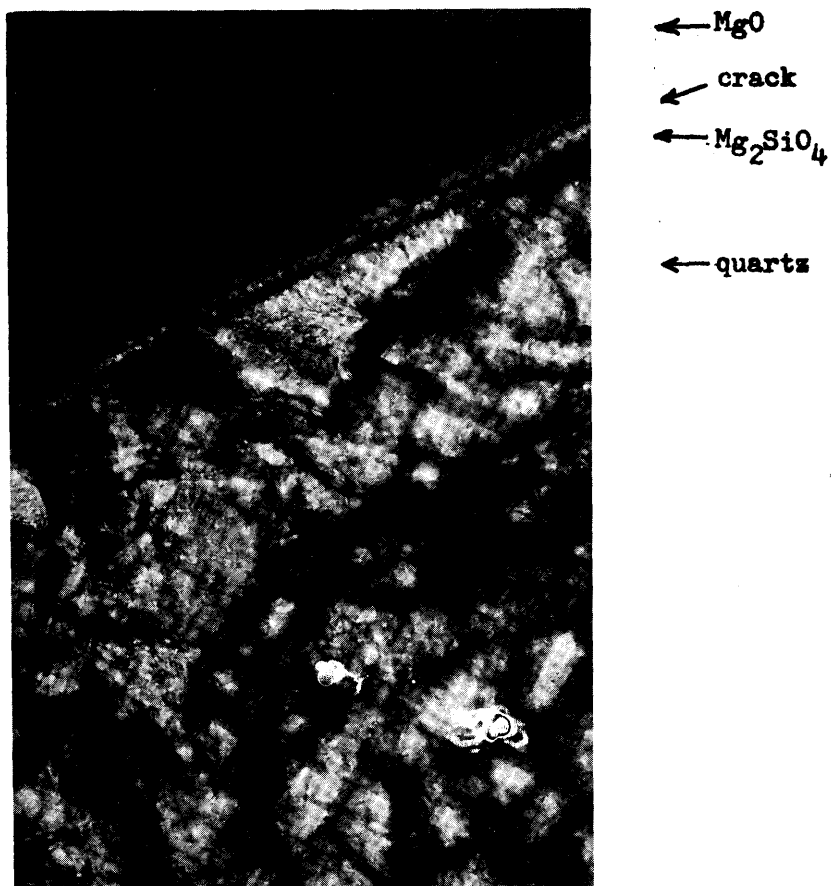


Figure IV-4 Thin section micrograph of MgO - quartz reaction interface on basal plane of quartz taken under crossed nicols. The specimen was heated at 1340 °C for 24 hours.

Figure IV-5 Point counts from an electron probe scan across the MgO - quartz interface. The reaction couple was heated at 1340 °C for 24 hours. The scan originated on the quartz and crossed the product layer and then into the crack. The average point counts taken from the standard Mg_2SiO_4 are shown for comparison.

MgO-SiO₂ INTERFACE SCAN

○ Mg counts

× Si counts

Mg counts on

Mg₂SiO₄ std.

Mg counts on

MgSiO₃ std.

Si Counts
on
MgSiO₃ std.

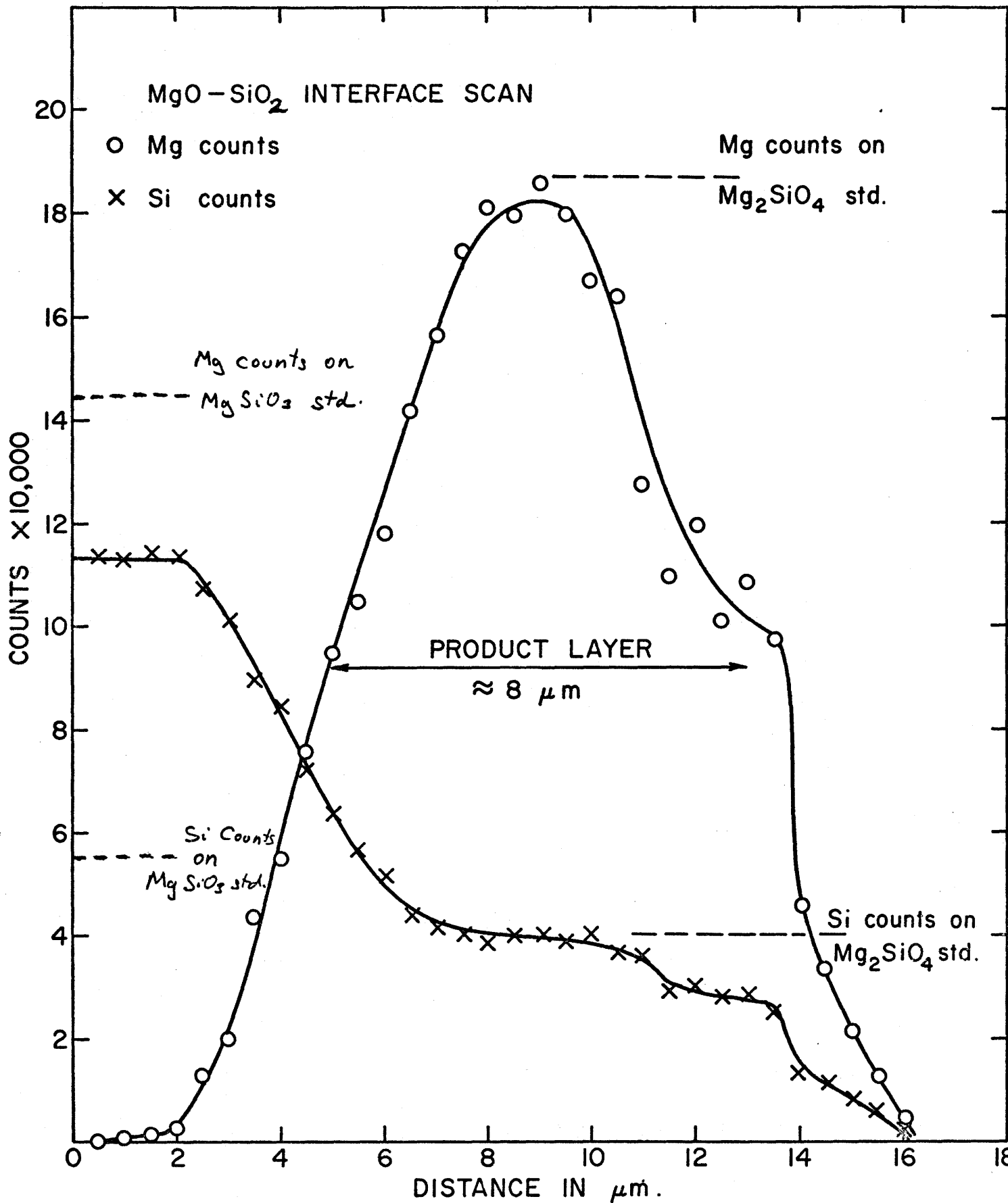
Si counts on
Mg₂SiO₄ std.

PRODUCT LAYER

≈ 8 μm

COUNTS × 10,000

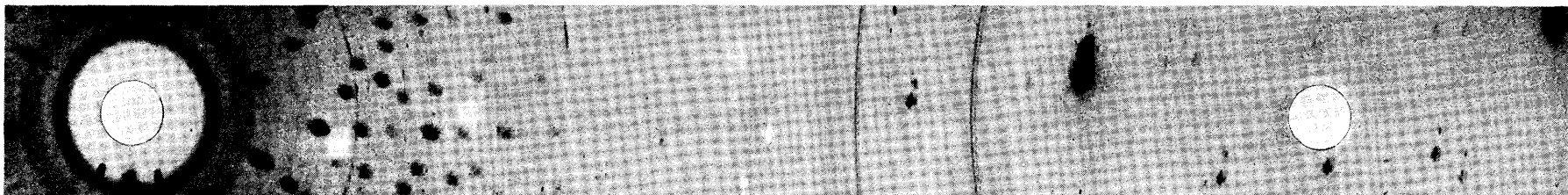
DISTANCE IN μm.



quartz, crosses the product layer and ends in the crack between the product layer and MgO. Comparison of the electron probe counts of the product layer with the counts of the forsterite and enstatite standards indicate that the product layer is predominately forsterite. Because of the poor electron stopping power of the reactant and product phases, the resolution was low, rendering it impossible to determine whether or not enstatite also exists in the product layer.

Attempts to obtain collaborating X-ray evidence were unsuccessful. Debye-Scherrer patterns of samples reacted at 1340°C for 24 hours showed the single crystal spot pattern for quartz, plus the powder pattern for MgO and other definite lines not corresponding to those of forsterite or any of the known polymorphs of enstatite or silica reported in the ASTM powder pattern file. X-ray patterns on three different samples heated at 1340°C for 24 hours gave similar results. In order to obtain X-ray data from a thicker product layer, a Debye - Scherrer pattern was taken of a sample heated at 1450°C for 24 hours. The lines produced in this pattern identified cristobalite, clino - enstatite, and forsterite, plus unidentifiable lines similar to those found in the previous experiments. Although no quantitative work was done to determine the ratio of clino-enstatite to forsterite, the intensity of the clino-enstatite lines were the stronger, lending support to Daengen 's findings that clino-enstatite is the major product formed in the temperature range 1450°C - 1500°C. The Debye-Scherrer patterns produced from the samples reacted at 1340°C and 1450°C are shown in Figures IV-6a and IV-6b. The corresponding spacings, along with those of clino-enstatite, forsterite, cristobalite, and MgO are given in Table IV-1. The d-spacings and intensity ratios of protoenstatite is given in Appendix III. The lack of a definite

forsterite or an enstatite pattern in the reaction samples heated at 1340°C does not constitute a proof that these compounds do not exist in the samples. Both forsterite and enstatite may exist in the product layer, however the thickness of the product layer or the size and orientation of the product grains may be such that a clear X - ray pattern will not form. One may only speculate as to the origins of the undefinable lines found in those Debye - Scherrer patterns. Three explanations are possible, i.e.



↑
264

Figure IV-6a The Debye - Scherrer Pattern taken of the quartz pellet after reacting with MgO at 1340 °C for 24 hours.

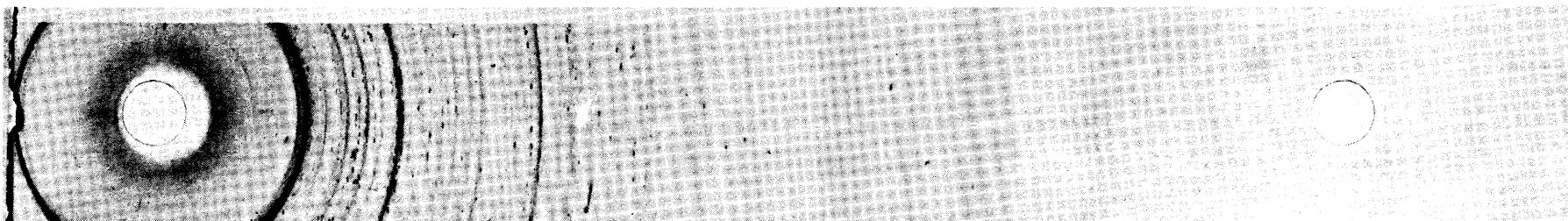


Figure IV-6b The Debye - Scherrer Pattern taken of the quartz pellet after reacting with MgO at 1450 °C for 24 hours.

Table IV-1 Debye - Scherrer X-ray patterns obtained from couples reacted at 1340 °C and 1450 °C for 24 hours. The ASTM powder pattern cards for Clino - enstatite, Forsterite, Cristobalite, and MgO are also given.

1340 °C		1450 °C		Clino - enst.		Forsterite		Cristobalite		MgO	
d	I	d	A I	d	A I/I°	d	A I/I°	d	A I/I°	d	A I/I°
6.02	Mc	6.28	Wc	6.36	4						
		5.09	Ws			5.11	26				
		4.27	Mc	4.28	8						
		4.06	Sc					4.05	100		
3.59	Ws	3.88	Ws			3.88	69				
		3.49	Mc			3.49	21	3.53	3		
		3.41	Ws								
		3.26	Ms	3.29	50						
3.12	Ms	3.16	Ms	3.17	60						
		3.15	Mc					3.14	11		
		3.02	Ms			3.00	17				
		2.98	Ms	2.98	95						
2.64	Ss	2.87	Ms	2.88	100						
		2.85	Mc					2.84	13		
		2.75	Ms			2.77	53				
		2.68	Ms								
2.52	Ws	2.55	Ws	2.54	35						
		2.49	Ms	2.51	73						
		2.48	Mc					2.48	20		
		2.45	Ss	2.46	60	2.46	100				
		2.38	Wc								
		2.29	Ws			2.27	59				
2.18	Ms	2.26	Ws			2.25	33				
		2.20	Ms	2.21	20						
		2.12	Ms	2.12	45					2.11	100
		2.07	Ws								
2.01	Ms	2.02	Ms	2.02	10	2.03	5				
1.75	Mc	1.97	Ws	1.97	4	1.95	5				
		1.93	Mc					1.93	5		
		1.88	Mc			1.88	5	1.87	7		
		1.74	Ws	1.73	16	1.74	60				
1.70	Wc	1.70	Wc					1.69	3		
1.67	Wc	1.67	Wc			1.67	13				
1.64	Wc	1.64	Ss			1.64	12				
1.62	Wc	1.60	Ss			1.61	15				
1.49	Sc									1.49	52
1.44	W										
1.40	W										
1.35	W										
1.32	W										
1.27	Sc									1.27	4
1.22	Sc									1.22	12
1.05	Mc									1.05	5
.967	Wc									.967	2
.942	Sc									.942	17
.860	Sc									.860	15

Legend : W = weak M = medium S = strong

c = continuous s = spotty

- 1) a meta - stable phase of silica has formed as β - quartz transforms to cristobalite.
- 2) the pattern of quartz or cristobalite has shifted to a significant degree due to the diffusion of magnesium and oxygen ions into the silica.
- 3) the product layer contains a meta - stable polymorph of forsterite.

Two other phases of forsterite have been described by Suito ⁽⁵²⁾.

Although they are high pressure forms, they may grow by an epitaxial mechanism from the β - quartz. It has not been possible to obtain X - ray patterns of these high pressure polymorphs for comparison with the observed patterns.

IV.2 Kinetic Data

Plots of product layer thickness² versus time on both the basal (0001) and the prism ($10\bar{1}0$) planes of β - quartz for the reaction in wet and dry nitrogen are shown in Figures IV - 7 to IV - 12. No significant difference was found in the reaction rate on the basal and prism planes of quartz. The results follow the parabolic rate law.

$$x^2 + x_0^2 = 2k_p t \quad (12)$$

where $x_0^2 = \text{constant}$.

The values of $2k_p$ and x_0^2 , determined by linear regression analysis, at various temperatures and water vapor pressures are given in Table IV - 2.

The kinetic data for the reaction between β - quartz and MgO in wet atmospheres of 45, 135, and 250 mm Hg water partial pressure was also plotted parabolically. The results showed that water vapor had a marked

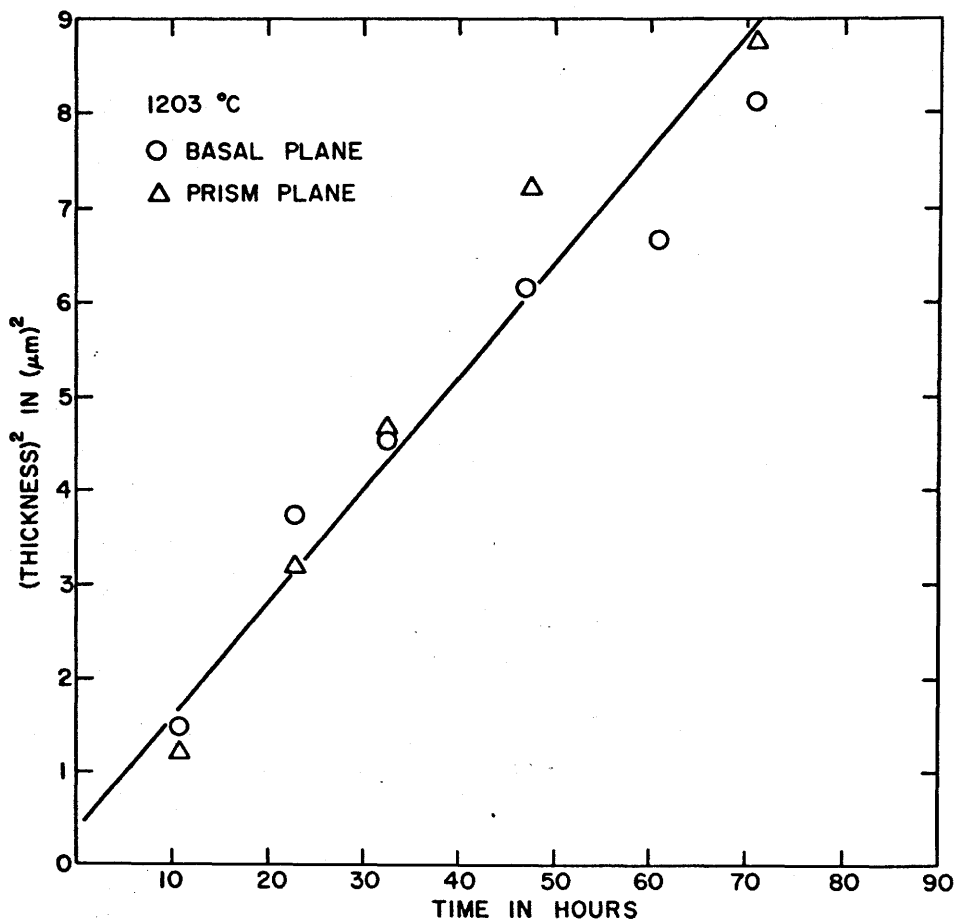


Figure IV-7 The growth of Mg_2SiO_4 at 1203 °C on both the basal and prism planes of quartz.

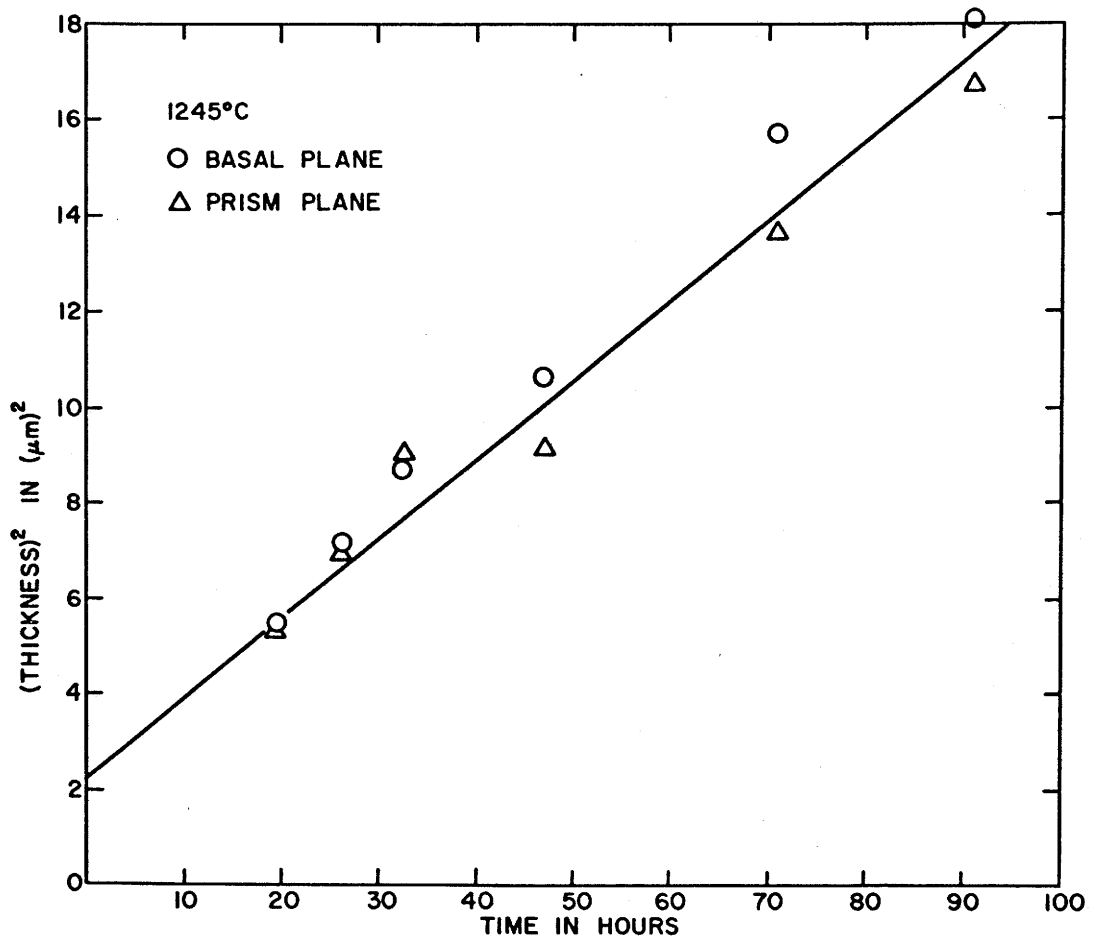


Figure IV-8 The growth of Mg_2SiO_4 on both the basal and prism planes of quartz at 1245 °C.

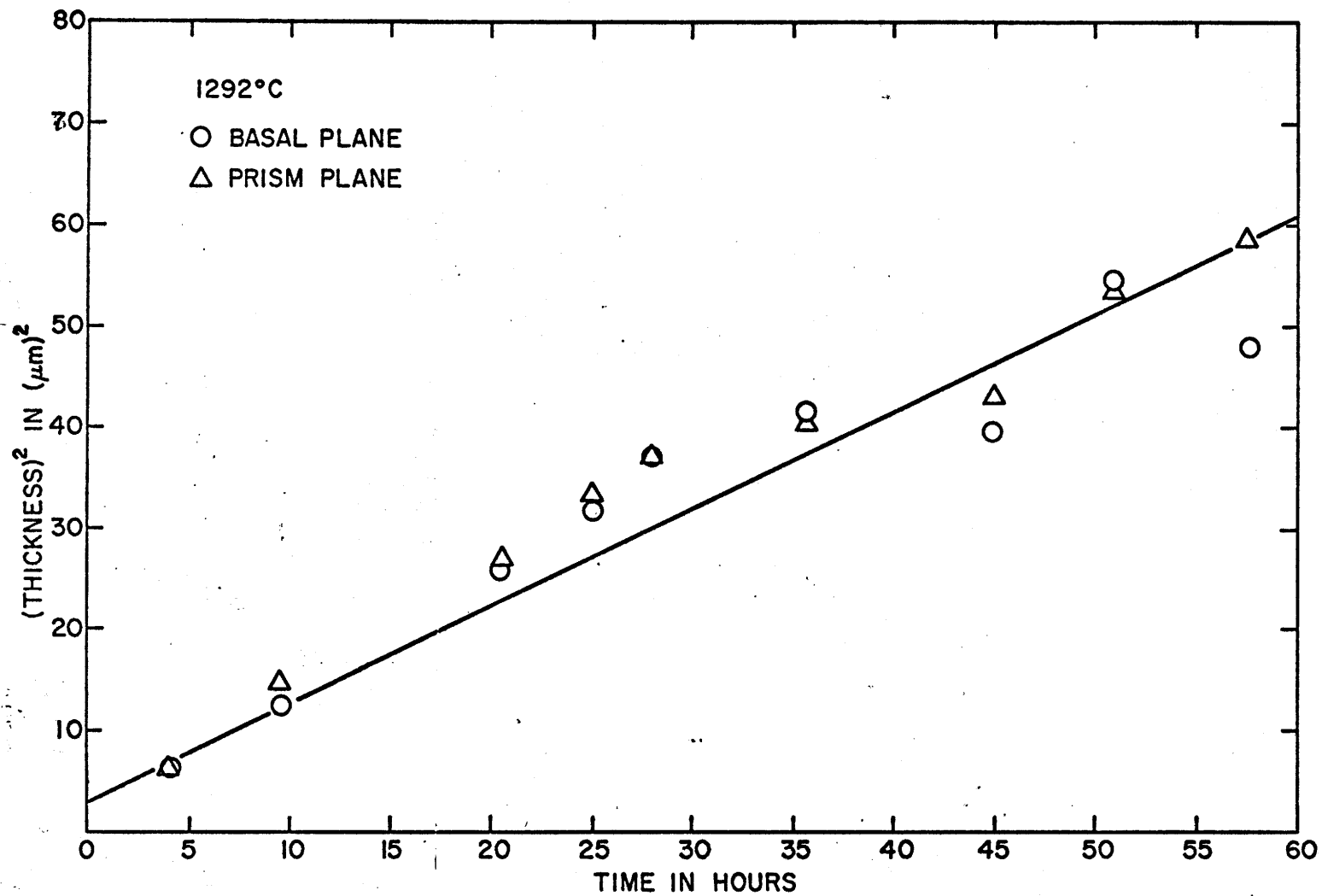


Figure IV-9 The growth of Mg_2SiO_4 on both the basal and prism planes of quartz at 1292 °C.

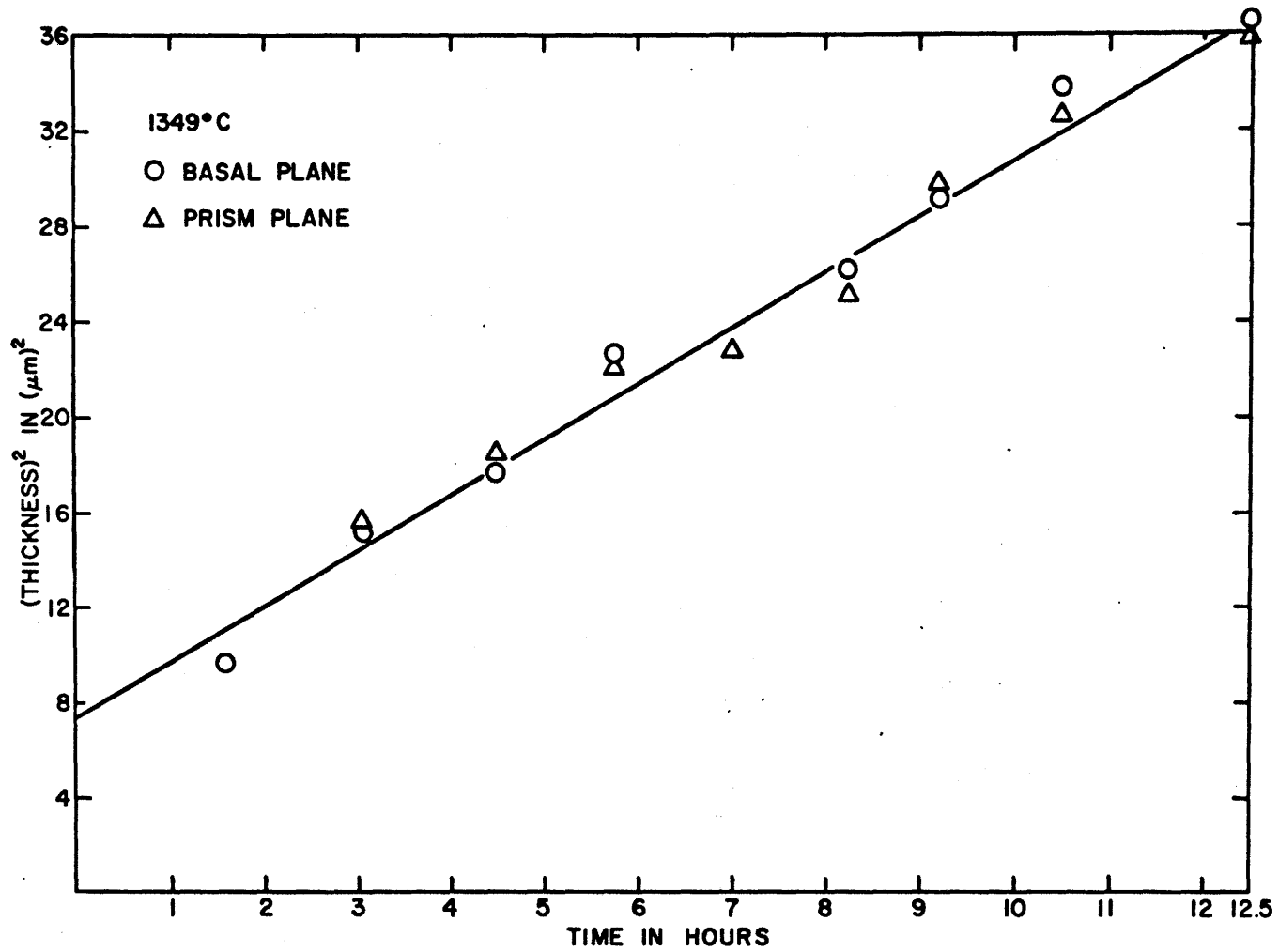


Figure IV-10 The growth of Mg_2SiO_4 on both the basal and prism planes at 1349 °C.

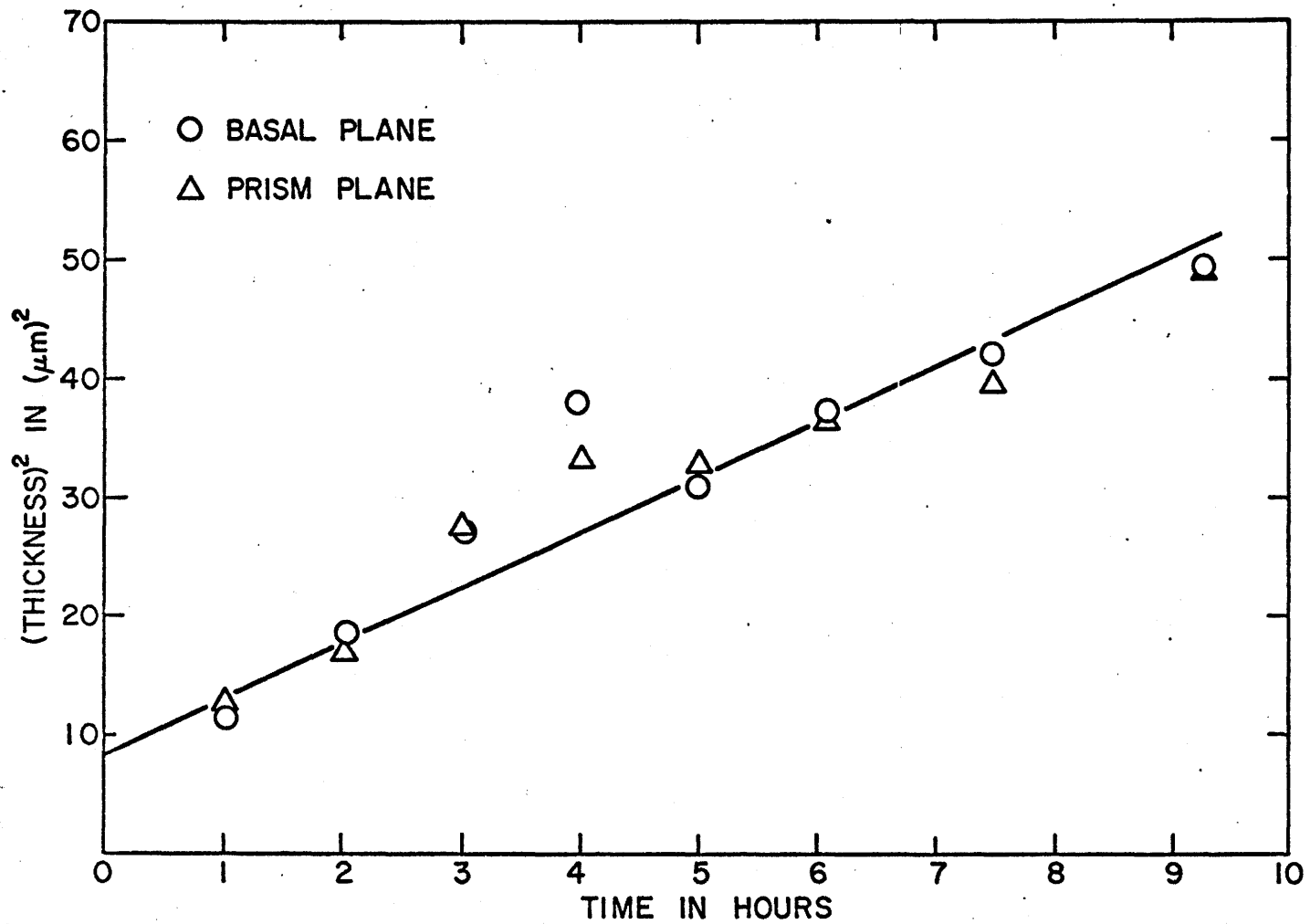


Figure IV-11 The growth of Mg_2SiO_4 on the basal and prism planes of quartz at 1415 °C.

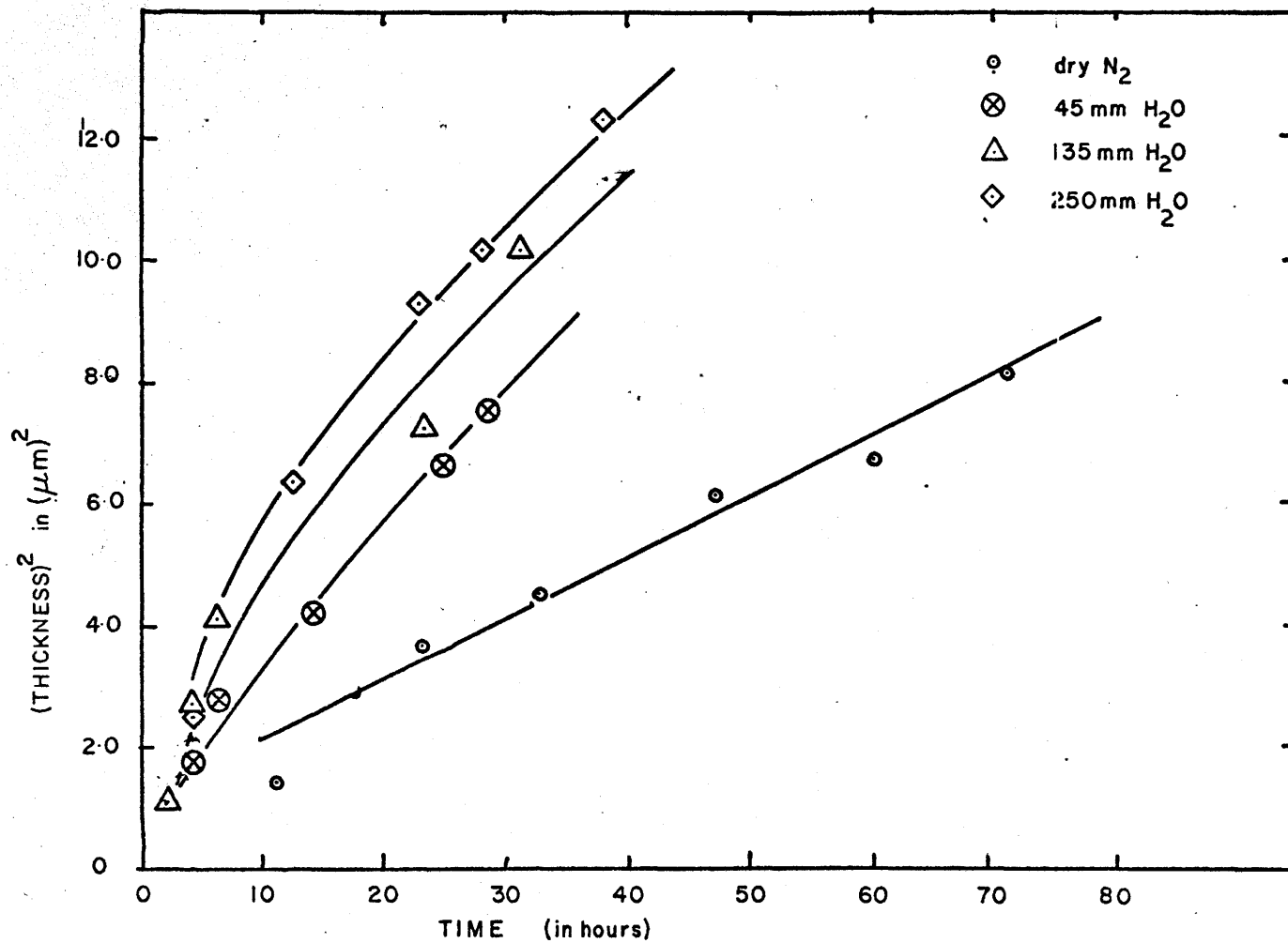


Figure IV-12 The rate of growth of Mg_2SiO_4 in atmospheres containing 45, 135, 250 mm Hg water partial pressure compared with the rate of growth in dry atmosphere.

Table IV-2

Parabolic Data for the Reaction Between MgO - SiO₂

T in °C	$2k_p (\mu\text{m}^2/\text{hr})$	$x_p^2 (\mu\text{m}^2)$
1203	.112	.661
1245	.164	2.68
1292	.827	8.23
1349	2.33	7.34
1415	4.10	11.9
1200, 45 mm H ₂ O	.220	1.25

influence leading to an increase of the reaction rate. Increasing the partial pressure of the water vapor increased the reaction rate, and at the same time greater deviations from the parabolic rate law were observed. The influence of the water vapor is shown in Figure IV - 12.

The validity of the parabolic rate law for a system can be verified by plotting the data on a log-log plot. For an ideal growth law, the equation of product growth will be,

$$x^n = nk_p t + \text{Constant} \quad (31)$$

where $n = 1$ for the linear rate law

$n = 2$ for the parabolic rate law

$n = \dots$ and so on

Making the assumption that the Constant $\ll nk_p t$, an assumption which is valid after a relative short reaction period, it is possible to take the logarithms of both sides of the equation.

$$\log x = k' + \frac{1}{n} \log t \quad (32)$$

The data for the wet and dry runs are given in Figures IV - 13 and IV - 14. These results indicate some deviation from the ideal parabolic law where $\frac{1}{n} = 0.5$. The initial non - parabolic period, which can be noticed in the product layer thickness² vers. time graphs (Figures IV - 7 through IV - 12), or less - than - ideal contact between the reactants, could cause $\frac{1}{n}$ to be less than $\frac{1}{2}$. If the rate - determining step is the reaction at the SiO₂ - product interface and not the diffusion of the reactants through the product layer, the rate of growth of the product would follow the linear law⁽³⁵⁾, $x + x_0 = kt$, resulting in the value of $\frac{1}{n}$ to be closer to one. The observed results at least indicate that the reaction is not controlled by the rate

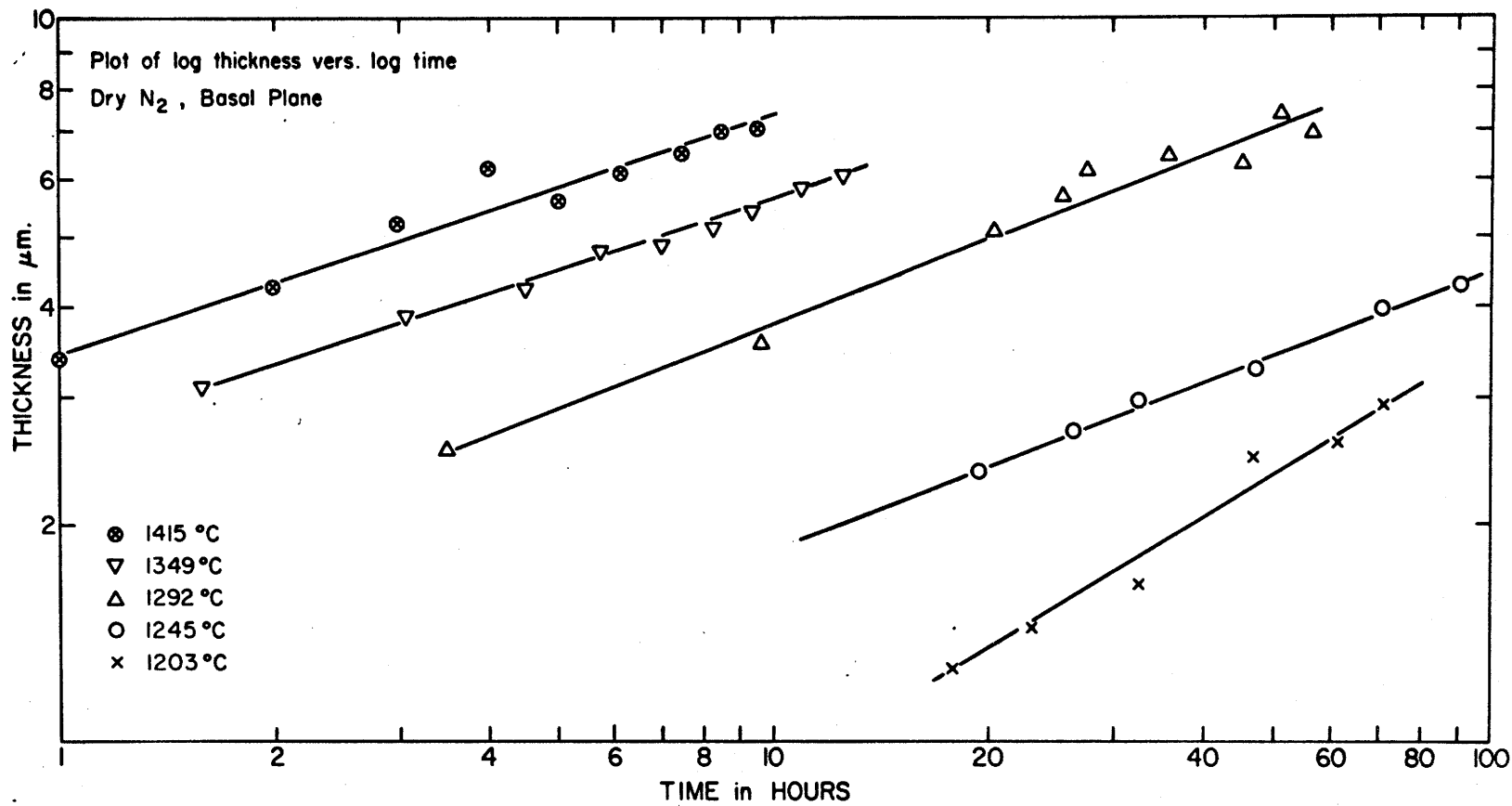


Figure IV-13 The plot of log product layer thickness vers log time for the growth of Mg_2SiO_4 at 1203, 1245, 1292, 1349, and 1415 °C.

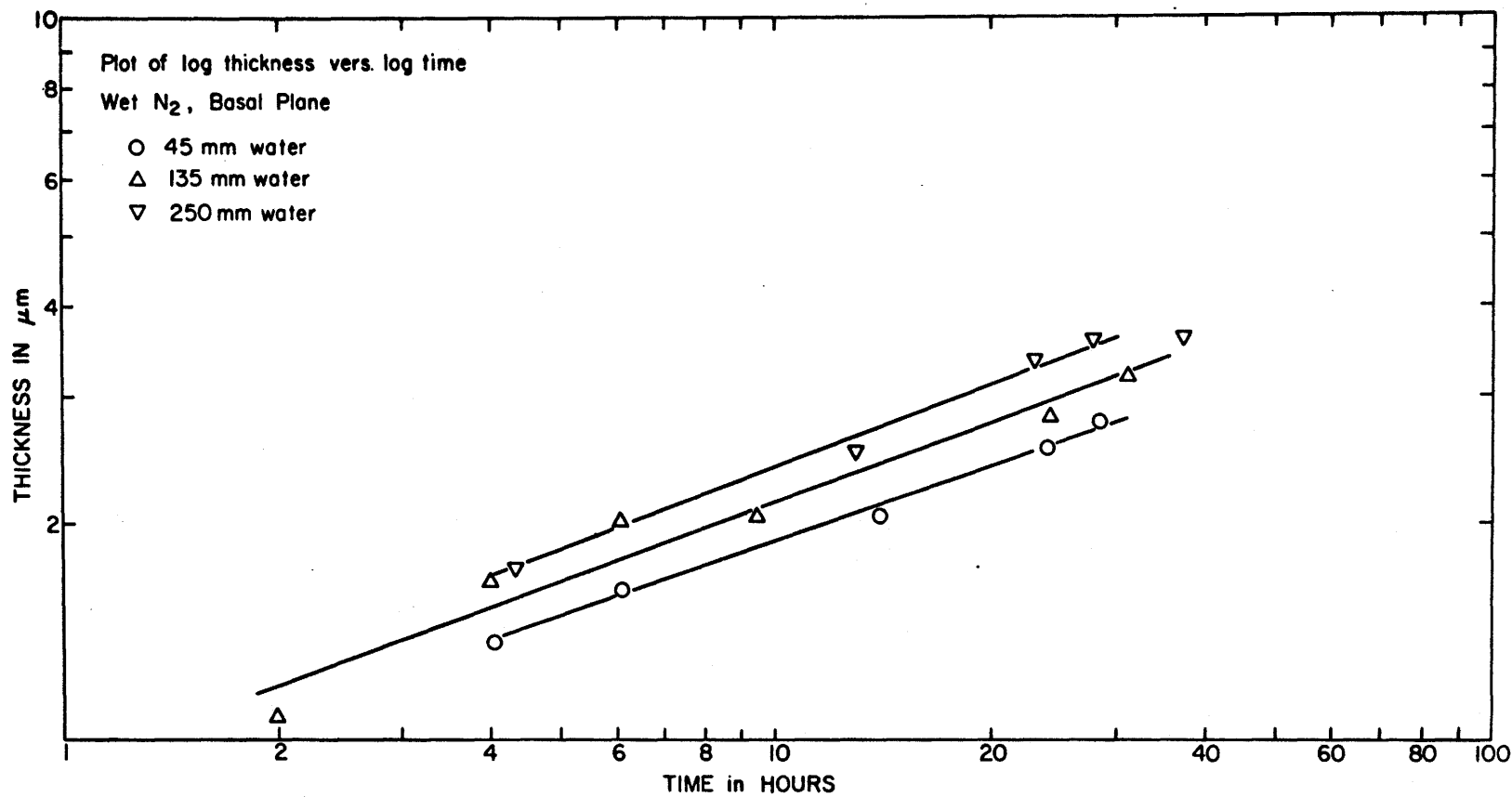


Figure IV-14 Plot of log product layer thickness vers log time at 1200 °C with 45, 135, and 250 mm Hg water vapor pressure.

Table IV-3

Slopes of the Log - Log - Plots for the Reaction
Between β - quartz - MgO

T in °C	P _{H₂O} (mm Hg)	$\frac{1}{n}$
1203	0	.60
1245	0	.38
1292	0	.38
1349	0	.32
1415	0	.33
1200	45	.34
1200	135	.36
1200	250	.34

of reaction at the product reactant interface.

The traditional relationship between the rate constant and the activation energy is in the form of,

$$k = k_0 \exp(-\Delta E/RT) \quad (33)$$

In solid state reactions, the dependence of k on T is more complex. From equation 26, it can be seen that k_p itself is a function of $\frac{1}{T}$, while G° is a linear function of T and \bar{D}_i has an exponential dependence of $\frac{1}{T}$ in the form of (36),

$$\bar{D}_i = \bar{D}_i^\circ \exp(-\Delta E/RT) \quad (34)$$

The activation energy of the reaction will be determined by the equation

$$\frac{k_p RT}{\delta \Delta G} = \bar{D}_i^\circ \exp(\Delta E/RT)$$

The plot of $\log(k_p T)$ versus $\frac{1}{T}$ is shown in Figure IV-15. The value of ΔE , as determined by linear regression, is 101 kcal/mole. This compares with the activation energy, as defined by equation 33, obtained by Brindley and Hayami of 78 kcal/mole and by Hayami and Ogura of 92 - 110 kcal/mole for the reaction $2\text{MgO} + \text{SiO}_2 \longrightarrow \text{Mg}_2\text{SiO}_4$. The activation energy for the reaction $\text{MgO} + \text{MgSiO}_3 \longrightarrow \text{Mg}_2\text{SiO}_4$ is given as 106 kcal/mole by Hayami and Ogura. The similarity of the activation energies of the formation of forsterite from enstatite and magnesium oxide, and the formation of forsterite from silica and magnesium oxide indicates that the rate controlling step involves a similar mechanism.

IV.3 The Reaction Mechanism

From the location of the reaction layers, the reaction mechanism must be one of Mg^{2+} and O^{2-} transport across the product layer. As listed

in Table II-2, the possible mechanisms are;

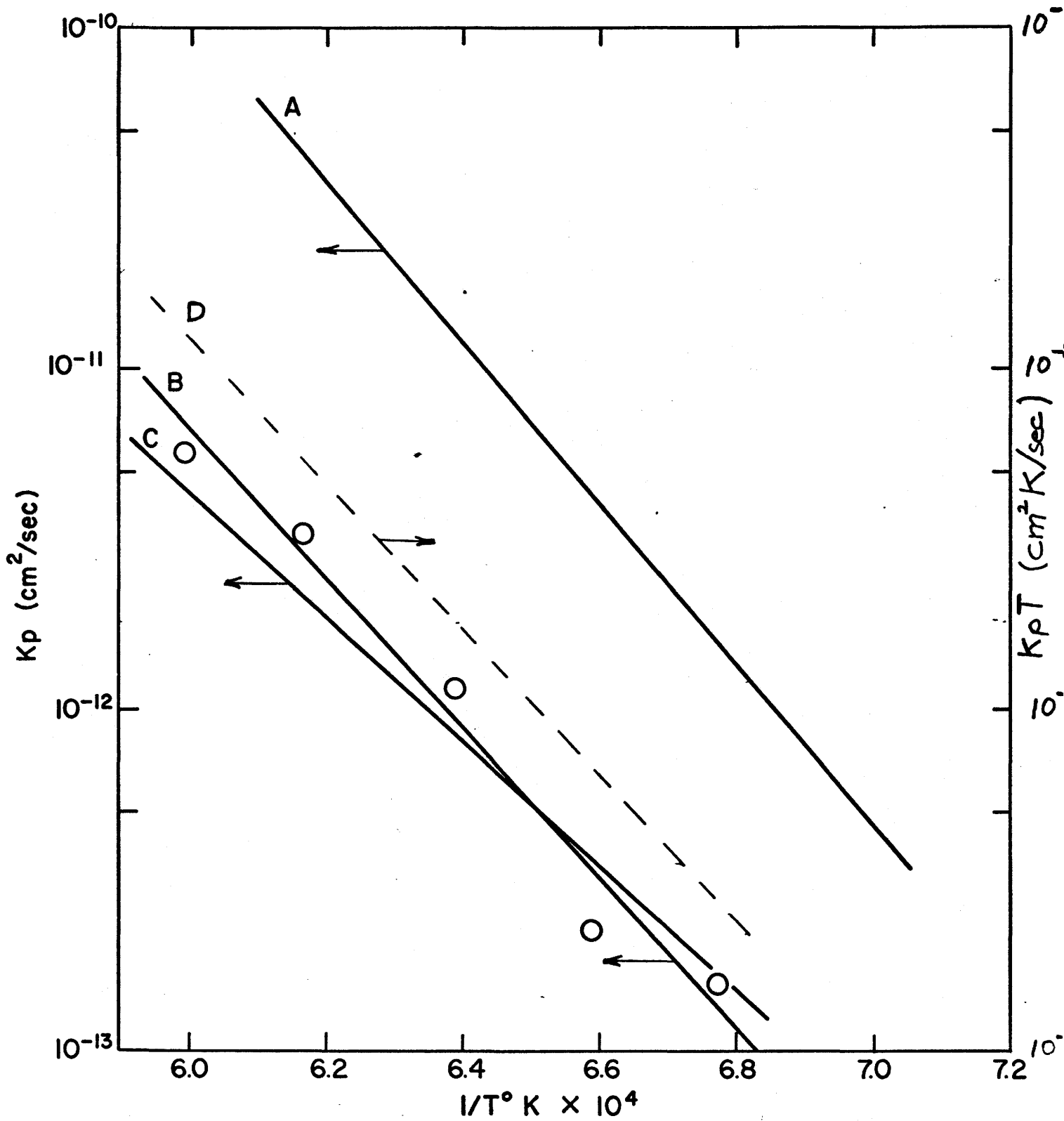
- 1) $D_{Mg} > D_O > D_{Si}$, $\gamma = 1$, the rate controlling step is O^{2-} diffusion through the product layer.
- 2) $D_O > D_{Mg} > D_{Si}$, $\gamma = \frac{1}{2}$, the rate controlling step is Mg^{2+} diffusion through the product layer.
- 3) gas phase transport of oxygen and Mg^{2+} and e^- diffusion through the product layer.

The gas phase mechanism is unlikely for two reasons, i.e. the mechanism requires that no barriers to gas transport exist across the product layer, and also that some oxygen gas exists in the atmosphere surrounding the reaction. Experiments by Daemgen⁽²³⁾ showed that varying the oxygen partial pressure surrounding the reaction samples from 1 to 10^{-12} atm. did not change the reaction rate. The gas phase mechanism also requires forsterite to be an electronic conductor, which is not likely at temperatures below 1500 °C. Hence, the growth of forsterite must be by a mechanism of ionic diffusion.

In order to distinguish whether the mechanism is Mg^{2+} or O^{2-} diffusion controlled, relevant diffusion data is required. The diffusion of Mg^{2+} in Mg_2SiO_4 in equilibrium with MgO and with $MgSiO_3$ was studied by Pluschkell^(19,37). At 1300 °C, D_{Mg} for Mg_2SiO_4 in equilibrium with MgO was approximately 10^{-11} cm²/sec, while D_{Mg} in equilibrium with $MgSiO_3$ was approximately 10^{-9} cm²/sec. There are no reported values for oxygen diffusion in Mg_2SiO_4 . Co_2SiO_4 appears to be the only silicate for which oxygen diffusion has been measured. Tracer diffusion on Co_2SiO_4 at 1220 °C at $P_{O_2} = 300$ torr gave D_O as 10^{-14} cm²/sec⁽³⁷⁾. This value serves only as a reference to give an order of magnitude value for

Figure IV-15 Activation energy plots for reactions in the MgO - SiO₂ system.

- A) rate constant for reaction $\text{MgSiO}_3 + \text{MgO} \rightarrow \text{Mg}_2\text{SiO}_4$
from Hayami and Ogura.
- B) best straight line own data for reaction
 $2\text{MgO} + \text{SiO}_2 \rightarrow \text{Mg}_2\text{SiO}_4$.
- C) rate constant for reaction $2\text{MgO} + \text{SiO}_2 \rightarrow \text{Mg}_2\text{SiO}_4$
determined by Brindley and Hayami.
- D) best fit straight line of $\log(k_p T)$ versus $\frac{1}{T}$
of own data for reaction $2\text{MgO} + \text{SiO}_2 \rightarrow \text{Mg}_2\text{SiO}_4$.



D_0 in Mg_2SiO_4 . The diffusion coefficient of the rate determining diffusing species is given by

$$k_p = -\gamma \bar{D}_1 \frac{\Delta G^\circ}{RT} \quad (26)$$

Values of \bar{D}_1 have been calculated from measured k_p and thermodynamic data assuming $\gamma = 1$, for the case of oxygen diffusion being the rate controlling step, and $\gamma = \frac{1}{2}$ for the case of magnesium being the rate controlling diffusing species. Table IV-4 shows these calculated values. Comparing the values of \bar{D}_1 in the column under $\gamma = 1$, (or under $\gamma = \frac{1}{2}$), it can be seen that the average diffusion coefficient of the rate controlling species is much less than the measured value of D_{Mg} in forsterite, and approximately the same order as D_0 in Co_2SiO_4 . This evidence tends to support oxygen diffusion as the rate controlling step of the reaction, i.e. $D_{Mg} \gg D_0 \gg D_{Si}$.

It has been shown therefore that the product layer grows by Mg^{2+} and O^{2-} diffusion through the forsterite layer and the subsequent reaction at the β - quartz - product interface. It has however not proved possible to eliminate the possible existence of enstatite in the product layer. Enstatite was found as a reaction product by Daemgen⁽²³⁾ and by Brindley and Hayami⁽⁶⁾, who studied the reaction between MgO and SiO_2 under different conditions. The rate of growth on the ($1\bar{1}00$) and the (0001) planes of β - quartz has been shown to be identical, indicating that the product composition and orientation are similar on both planes. This latter fact is interesting when compared to the results of the β - quartz - CaO reaction. In this system, Burte⁽⁵¹⁾ found the rate of growth of Ca_2SiO_4 to be much greater on the (0001) plane of quartz, as compared to the rate on the ($1\bar{1}00$) plane. Figure IV-16 shows the increased rate of growth of Ca_2SiO_4 on the basal planes in both wet and dry atmospheres as found by Burte. The existence of this anisotropic effect in

Table IV-4

Diffusion Coefficients of Rate Controlling Species

T in °C	k_p cm ² /s X 10 ¹³	ΔG° kcal/mole	\bar{D}_i cm ² /s X 10 ¹⁴	$\gamma = 1$	\bar{D}_i cm ² /s X 10 ¹⁴	$\gamma = \frac{1}{2}$
1203	1.56	-15.5	2.96		5.92	
1245	2.24	-15.6	4.34		8.68	
1292	11.5	-15.6	22.8		45.6	
1349	32.4	-15.7	66.7		133.	
1415	57.0	-15.8	121.		242.	

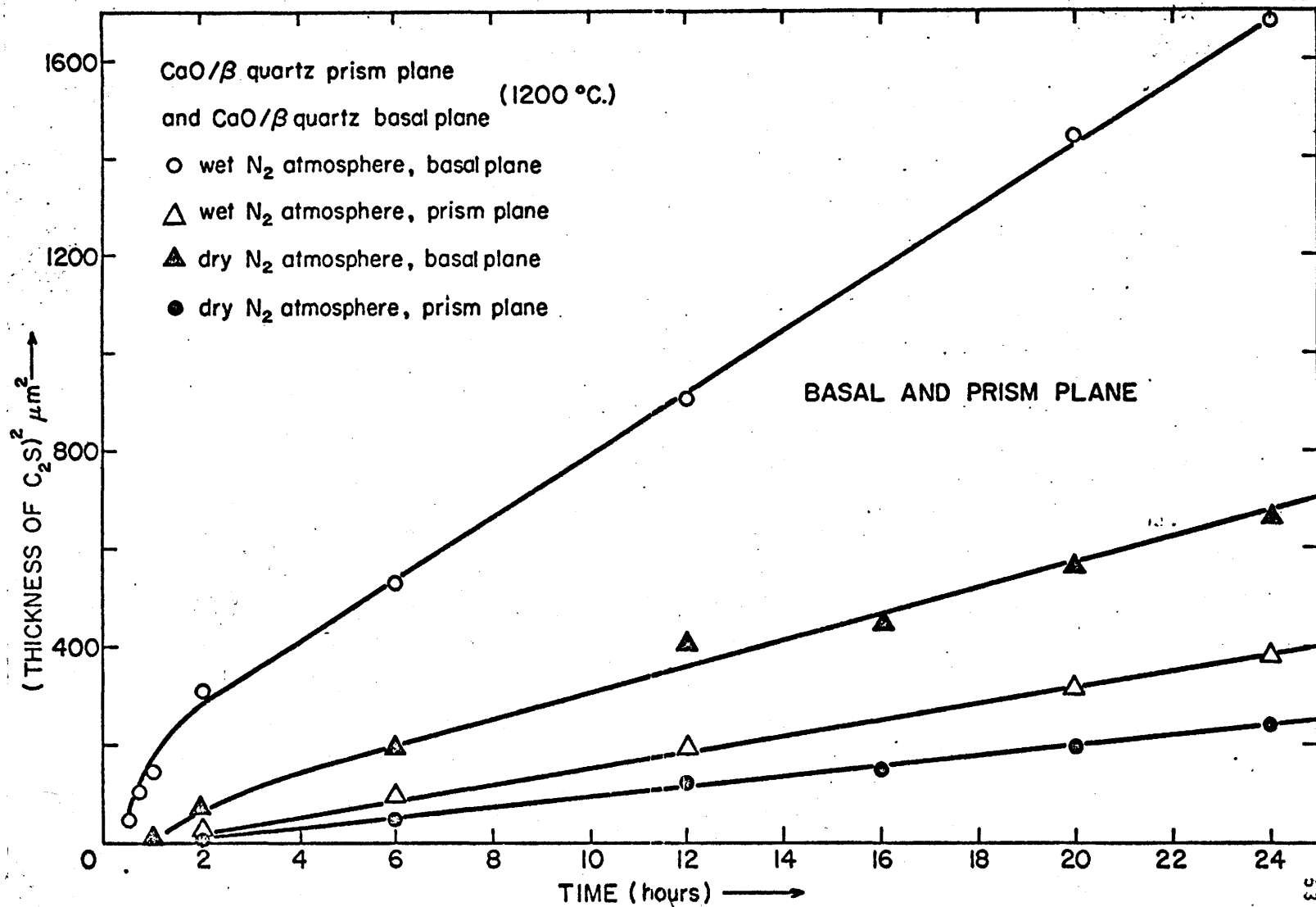
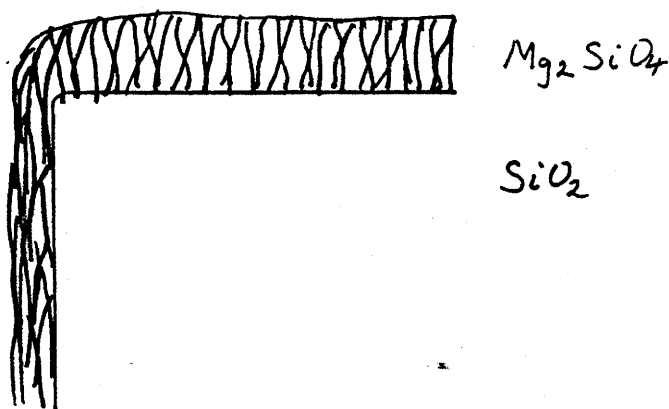


Figure IV-16 The anisotropy of Ca₂SiO₄ growth on the basal and prism planes of quartz in dry and wet nitrogen atmospheres.

the β - quartz - CaO system, and the lack of it in the β - quartz - MgO system is interesting. In order to attempt to understand what causes these two systems to differ, one should first discuss the three possible causes of this anisotropy, and their relevance to these two systems. A possible cause of anisotropy of the reaction rates is epitaxial growth of the product layer. Epitaxial growth means that the crystallographic orientation of the product phase is related to the orientation of the β - quartz plane from whence it grew. This might cause an increase in the reaction rate on one of the planes in two ways. If there is any anisotropy of the diffusion coefficients of the divalent cations in the product layer, the rate of fastest growth will be in the direction of the largest diffusion coefficient. Secondly, if the product crystallizes in a regular array of plate or needle like crystals, grain boundary diffusion will accelerate the growth rate in the direction of the plates or needles. This idea is clarified in the following sketch, where the relationship between product layer thickness and orientation of the product layer is shown. To determine whether or not the lattice parameters of β -



quartz and either α' - Ca_2SiO_4 or Mg_2SiO_4 match in some manner to allow epitaxial growth would be a very difficult exercise. However, in the β - quartz - MgO system, experimental evidence has shown that the product layer was the

same on both planes of quartz and it appeared to be in the form of randomly oriented fine crystallites which is not indicative of epitaxial growth. Burte did not discuss the orientation of the product layer in the β - quartz - CaO system.

If a nucleation step, or a rate controlling step involves the diffusion of divalent cations and anions into the quartz structure, an anisotropic effect might be observed. Frischat^(13,14,50) has noted that ionic species diffuse along the C - axis of quartz more rapidly than along the a - axis. The solubility of MgO in β - quartz was found to be negligible, and the rate controlling step has definitely been shown not to be a reaction controlled one, therefore this scheme is not operative in the β - quartz - MgO system. In the β - quartz - CaO system, Burte found the solubility of CaO in β - quartz to be appreciable and he believed the product layer formed by the diffusion of Ca^{2+} and O^{2-} into β - quartz, the building of Ca^{2+} and O^{2-} concentrations to some critical level, and finally the nucleation of the Ca_2SiO_4 product. The Ca^{2+} anion is known to diffuse more rapidly parallel to the C - axis than a - axis of quartz⁽⁵⁰⁾. Burte suggested that this may be the cause of the anisotropy of the Ca_2SiO_4 growth.

A third possible cause for the anisotropy in the β - quartz - CaO system is the formation of different products, or products with different crystal structure on the basal or prism planes of quartz. In the β - quartz - MgO system, the major product was forsterite on both planes. The presence of enstatite could not be confirmed on either plane of quartz. In the β - quartz - CaO system, the major product was Ca_2SiO_4 , which occurs in two high temperature polymorphs, the α and α' form. Burte believed that α - Ca_2SiO_4 formed on the basal planes and α' - Ca_2SiO_4 formed on the prism plane of quartz.

Differences in the diffusivities of Ca^{2+} and O^{2-} in the α and α' polymorphs of Ca_2SiO_4 could lead to anisotropy of the product growth.*

Because of the suspected fine grain size of the product layer, the role of grain boundary diffusion cannot be discounted as the method of reactant transport across the product layer. In the $\text{PbO} - \text{SiO}_2$ system, Hardel and Strocka⁽³⁸⁾ found that the rate of Pb_2SiO_4 growth is dependent on the size of the Pb_2SiO_4 crystallites, indicating that diffusion occurs along grain boundaries and also dislocation pipes. A similar effect was observed by Borchardt and Schmalzried⁽¹⁷⁾, who showed that the grain boundary diffusion affected the rate of Co_2SiO_4 growth. The acceleration of the reaction rate, due to grain boundary diffusion will be most pronounced in very thin silicate layers. This mechanism may cause the initial non-parabolic period of growth observed in the present work. As the reaction time increases, many of these preferred paths will become progressively eliminated by a combination of annealing and grain growth. In thicker product layers therefore, volume diffusion should become increasingly predominant, resulting in the reaction following parabolic kinetics. This coupled with the electrical potential driving force, could result in the existence of a critical product layer thickness beyond which parabolic kinetics are followed.

The main anion defect in forsterite as shown in Table II-1 is $V_{\text{O}}^{\bullet\bullet}$; and in intrinsic forsterite, oxygen diffusion, and thus the rate of product growth, will depend on the concentration of this defect. Figure II-7 shows the dependence of $[V_{\text{O}}^{\bullet\bullet}]$ on the activity of SiO_2 . The activity of SiO_2 in the product, forsterite, may be changed by reacting $\text{MgO} - \text{MgSiO}_3$ couples instead of $\text{MgO} - \text{SiO}_2$ couples. This in effect reduces the silica activity in the forsterite product layer because forsterite in equilibrium with MgO and MgSiO_3 will have a lower silica activity than forsterite in equilibrium with MgO and

* Anisotropy is further discussed in Appendix IV.

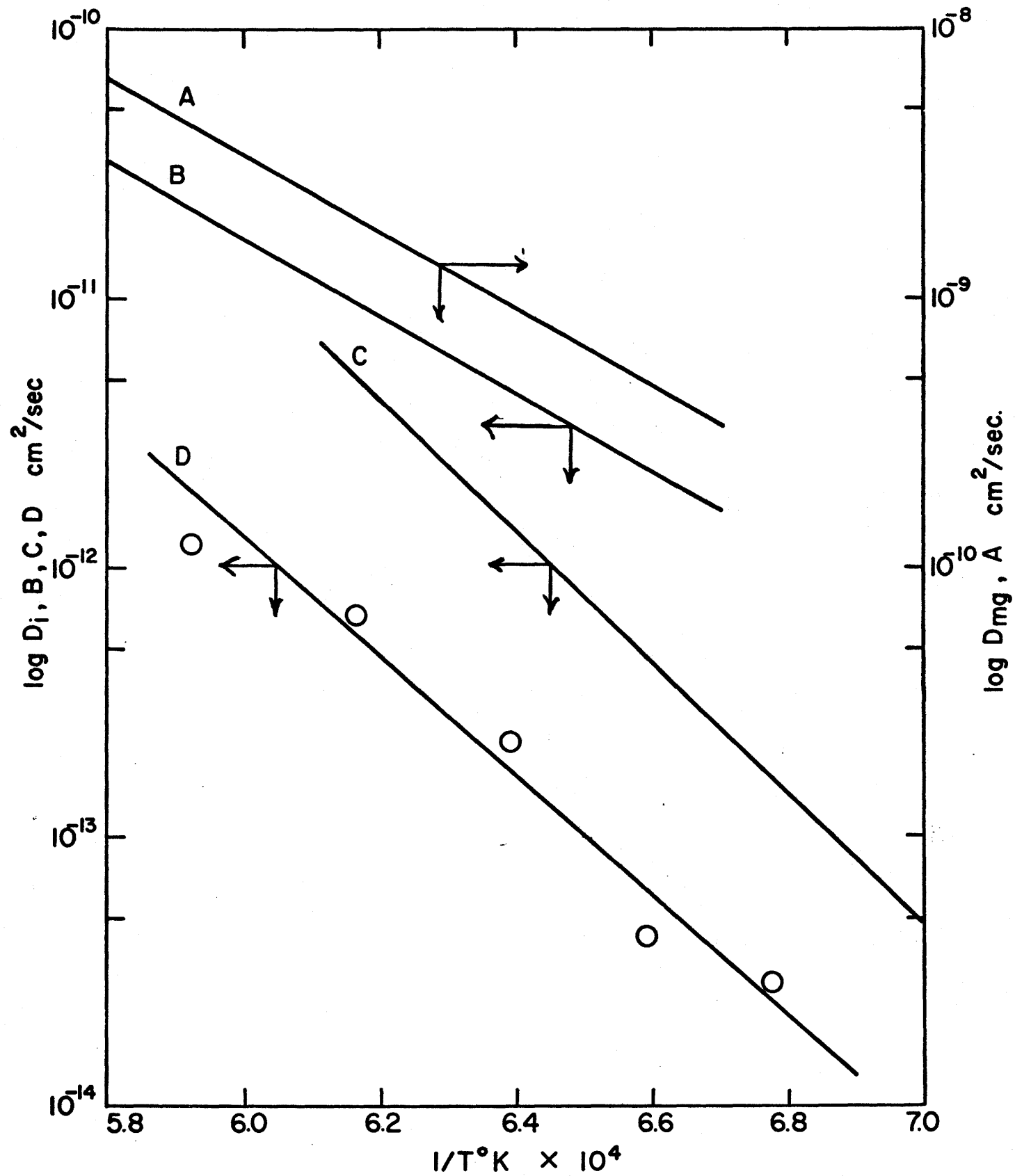
SiO₂.

Figure IV-17 shows the comparison between \bar{D}_O in Mg₂SiO₄ sandwiched between MgO and SiO₂, and \bar{D}_O in Mg₂SiO₄ sandwiched between MgSiO₃ and MgO. The latter value was calculated from the data of Hayami and Ogura⁽⁷⁾ using equation 17 with $\gamma = 4$ and $\Delta G^\circ = -7.3$ kcal/mole. Although caution must be exercised in comparing the two results, as they were obtained in different experiments, the dependence of \bar{D}_O on the activity of silica is clearly shown. As mentioned before, the average a_{SiO_2} in Mg₂SiO₄ is decreased when forsterite is formed from MgO - MgSiO₃ couples as compared with MgO - SiO₂ couples. The effect of decreasing the average a_{SiO_2} is an increased \bar{D}_O as shown in Figure IV-17 by lines C and D. Increasing the a_{SiO_2} in Mg₂SiO₄ has the opposite effect on D_{Mg} . There is a 100 fold increase in D_{Mg} in forsterite in equilibrium with MgSiO₃ compared with D_{Mg} in forsterite in equilibrium with MgO. It may be noted that there is no change in the activation energies of \bar{D}_O and D_{Mg} as the a_{SiO_2} changes. This is evidence that on the atomic scale, the mechanism of O²⁻ or Mg²⁺ diffusion does not change with varying a_{SiO_2} , but the number of sites available for "jumps" is effected. The high activation energy of \bar{D}_O , calculated from experimentally determined k_p 's, compared with D_{Mg} , which was measured by independent experiments should be noted. This confirms that the rate controlling diffusing species is not magnesium.

Little is known on how water vapor influences the defect structure of forsterite. In the forsterite structure, each silicon atom already has four oxygen atoms bonded exclusively to itself. To incorporate water into this structure, silicon may have to transfer from four to five coordination. The scheme of such an incorporation is shown in Figure IV-18a. The penta-coordinated silicon structure is in effect a method of stabilizing an oxygen interstitial in the forsterite structure. Such stability would involve the

Figure IV-17 The diffusivities of Mg^{2+} and O^{2-} in Mg_2SiO_4 under various conditions.

- A) Diffusivity of Mg^{2+} in Mg_2SiO_4 in equilibrium with MgSiO_3 .
- B) Diffusivity of Mg^{2+} in Mg_2SiO_4 in equilibrium with MgO .
- C) Diffusivity of O^{2-} in Mg_2SiO_4 calculated from the data of Hayami and Ogura.
- D) Diffusivity of O^{2-} in Mg_2SiO_4 calculated from own data.



dsp^3 hybrid state and may be valid because of the low energy d orbitals available for bonding. Compounds in which silicon is penta - coordinate have been reported⁽⁴²⁾. By the scheme shown in Figure IV-18a oxygen (or OH) has been formed in the interstitial sites. If electron bonding is readily broken by thermal energy, oxygen diffusion will accordingly be enhanced. The increased parabolic rate constant under wet conditions actually shows that the diffusivities of oxygen is increased in accordance with these considerations. In pure silica, water is thought to cause the breaking of the Si - O - Si bonds as shown in Figure IV-18b. The occurrence of hydroxyl groups in the network has been confirmed by infra - red spectroscopy⁽⁴³⁾.

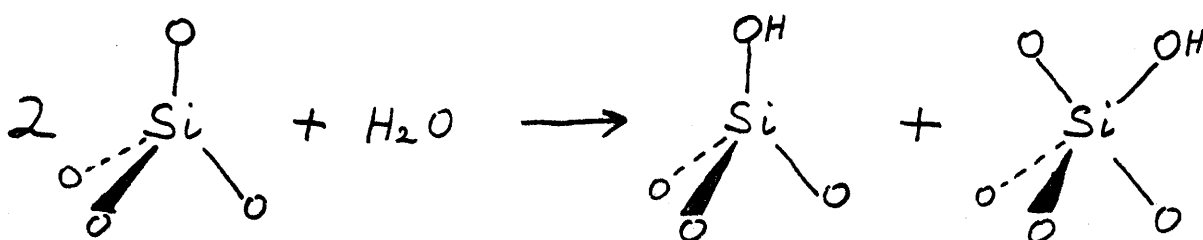


Figure IV-18a A possible mechanism for the incorporation of interstitial water in the olivine structure.

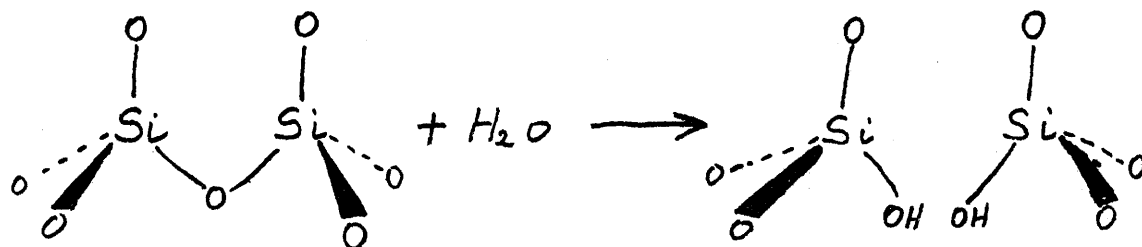
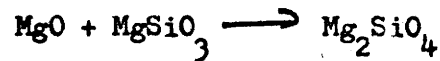


Figure IV-18b The mechanism of incorporation of interstitial water in pure silica.

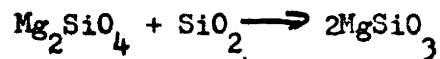
CHAPTER V

SUGGESTIONS FOR FUTURE WORK

In order to complete the study of the MgO - SiO₂ system, the reactions



and



should be studied using the method of this study. Both reactions are energetically favourable. The first reaction has already been studied in mixed powders by Hayami and Ogura⁽⁷⁾, but the second reaction has not yet been investigated from the point of obtaining kinetic data. Initial work on this topic would require some thought as to the possible reaction mechanisms, and what the corresponding values of β are, similar to that shown in Table II-2. One may study the first reaction by obtaining a single crystal of enstatite and embedding it in a MgO powder matrix. One may also use a single crystal MgO surrounded by a MgSiO₃ compact, but this is not recommended because the Mg²⁺ and O²⁻ will diffuse down the grain boundaries of MgSiO₃, giving erroneous results. The second reaction can be studied by surrounding a single crystal of silica in Mg₂SiO₄ powder. Tridymite or Cristobalite are the best polymorphs of silica to use because of the possible instability of β - quartz at reaction temperatures.

A few preliminary experiments have been carried out on these reactions by constructing couples of single crystal MgO surrounded by MgSiO₃ and of

β - quartz surrounded by Mg_2SiO_4 . These couples reacted at 1350 °C for 24 hours. In both cases, however, no reaction product formed. The reason for this is not evident; but it may be due to some nucleation barriers of the product layer.

CHAPTER VI
CONCLUSIONS

The following conclusions can be made from the work here presented.

1) The major reaction product for the reaction between β - quartz and MgO in the temperature range 1200 - 1400 °C is Mg_2SiO_4 .

2) The rate of formation of Mg_2SiO_4 closely follows parabolic reaction kinetics.

3) The reaction proceeds by Mg^{2+} and O^{2-} diffusion through the product layer with O^{2-} diffusion as the rate controlling step.

4) There is no difference between the reaction rates on the basal and prism planes of quartz.

5) Mg_2SiO_4 was found to be the major product formed in the temperature range 1200 - 1400 °C. The presence of $MgSiO_3$ is thermodynamically feasible, and minor amounts of this silicate were found by the utilized X - ray techniques.

6) Water vapor enhances the rate of Mg_2SiO_4 formation equally on the basal and prism planes of quartz. A mechanism is advanced in which this increase is associated with the presence of interstitial oxygen and hydroxol ion.

7) At 1450 °C, both $MgSiO_3$ and Mg_2SiO_4 form as products.

In closing a comparison can be made with the mechanisms of formation of the other silicates. In almost all cases, the formation occurs by the

diffusion of the divalent cation and oxygen across the silicate layer, with Si^{4+} diffusion playing no role in the reaction. Examples of this scheme include Mg_2SiO_4 , Ca_2SiO_4 , Pb_2SiO_4 , Zn_2SiO_4 , and Sr_2SiO_4 . In only one silicate, Co_2SiO_4 has it been reported that silicon diffusion takes part in the reaction^(37,41). It may therefore be concluded that, in general, the stability of the SiO_4^{4+} tetrahedra renders it difficult for silicon, and to a lesser extent oxygen, to diffuse. The divalent cations are ionically bonded, and have an abundance of interstitial sites available for diffusion, therefore these cations can diffuse rapidly in the silicate systems. The evidence available supports the concept that, in most silicate systems, the rate controlling step is not the diffusion of the divalent cation.

APPENDIX I

KROGER - VINK DIAGRAM FOR FORSTERITE

Under constant temperature, pressure and p_{O_2} , the defect structure of forsterite will depend on the activity of SiO_2 . The dependence of various defect concentrations with the activity of SiO_2 can be shown on a Kröger - Vink diagram.

Using the general equation of Schmalzried and Wagner⁽⁴⁴⁾ in the form of

$$\partial \log(i) = n_i \partial \log a_{SiO_2} \quad (I.1)$$

it is possible to show how defect concentrations vary with $\log a_{SiO_2}$. A few examples will be calculated to describe this procedure.

In the intrinsic region, where $[Mg_{i,0}^{\bullet\bullet}] = [V_{Mg,0}^{\prime\prime}]$ is the major defect pair, one may write the mass and site balance equation as



The corresponding equilibrium constant will be

$$K_1 = \frac{1}{(Mg_i)(V_{Mg})} \quad (I.3)$$

$$\text{and } \log K_1 = - \log (Mg_i) - \log (V_{Mg}) \quad (I.4)$$

Differentiation with respect to $\partial \log a_{SiO_2}$ results in

$$0 = - \frac{\partial \log Mg_i}{\partial \log a_{SiO_2}} - \frac{\partial \log V_{Mg}}{\partial \log a_{SiO_2}} \quad (I.5)$$

and since $[Mg_{i,0}^{\bullet\bullet}] = [V_{Mg,0}^{\prime\prime}]$

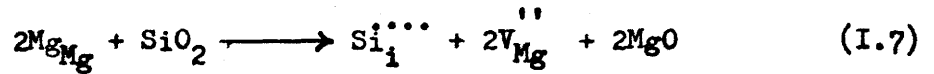
$$\frac{\partial \log V_{Mg,0}}{\partial \log a_{SiO_2}} = \frac{\partial \log Mg_{i,0}}{\partial \log a_{SiO_2}} = 0 \quad (I.6)$$

$$n_{V_{Mg,0}} = n_{Mg_{i,0}} = 0$$

This trivial case shows that the concentration of $V_{Mg,0}$ and $Mg_{i,0}$ is independent of a_{SiO_2} .

At increased activities of SiO_2 , the major defect pair will be

$$[Si_{i,T}] \equiv \frac{1}{2} [V_{Mg,0}^{''}]. \text{ Using the mass and site balance equation,}$$



with the corresponding equilibrium equation,

$$K_{II} = \frac{[Si_i] [V_{Mg}]^2 a_{MgO}^2}{a_{SiO_2}} \quad (I.8)$$

it is possible to calculate characteristic numbers n_i for $i = Si_i$ and $i = V_{Mg}$.

Using the integrated form of the Gibbs - Duhem equation,

$$a_{MgO}^2 \cdot a_{SiO_2} = \exp \Delta G^\circ / RT$$

and taking the log of both sides of equation I.8

$$\log K'_{II} = \log Si_i + 2 \log V_{Mg} - 2 \log a_{SiO_2}$$

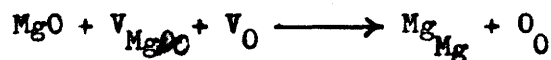
followed by differentiation with respect to $\log a_{SiO_2}$ yields

$$0 = \frac{\partial \log Si_i}{\partial \log a_{SiO_2}} + \frac{2 \partial \log V_{Mg}}{\partial \log a_{SiO_2}} - 2$$

Remembering that $[Si_i] = \frac{1}{2} [V_{Mg}]$, one gets

$$n_{Si_i} = \frac{\partial \log Si_i}{\partial \log a_{SiO_2}} = 2/3, \text{ and } n_{V_{Mg}} = \frac{\partial \log V_{Mg}}{\partial \log a_{SiO_2}} = 2/3$$

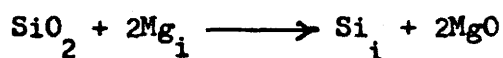
A similar set of calculations can be made at even higher activities of SiO_2 . $[V'_0] = [V_{\text{Mg},0}]$ will be the predominate defect pair. Using the mass balance equation,



one can show that

$$n_{V_0} = \frac{\partial \log V_0}{\partial \log a_{\text{SiO}_2}} = \frac{1}{4}, \text{ and } n_{V_{\text{Mg},0}} = \frac{\partial \log V_{\text{Mg},0}}{\partial \log a_{\text{SiO}_2}} = \frac{1}{4}$$

It is now possible to find the characteristic numbers of the defects Si_{Mg} , Si_i , V_0 , Mg_i throughout the range of silica activities in terms of $n_{V_{\text{Mg}}}$. For example, using the mass balance equation,



one will obtain,

$$n_{\text{Si}_i} = \frac{\partial \log \text{Si}_i}{\partial \log a_{\text{SiO}_2}} = 2 - 2n_{V_{\text{Mg}}}$$

The other defect characteristic numbers can be calculated in a like manner. These are found to be,

$$n_{\text{Si}_{\text{Mg}}} = \frac{\partial \log \text{Si}_{\text{Mg}}}{\partial \log a_{\text{SiO}_2}} = 2 - n_{V_{\text{Mg}}}$$

$$n_{V_0} = \frac{\partial \log V_0}{\partial \log a_{\text{SiO}_2}} = \frac{1}{2} - n_{V_{\text{Mg}}}$$

$$n_{\text{Mg}_i} = \frac{\partial \log \text{Mg}_i}{\partial \log a_{\text{SiO}_2}} = -n_{V_{\text{Mg}}}$$

With these equations, the Kröger - Vink diagram shown in Figure II-7 was calculated.

APPENDIX II

PREPARATION OF FORSTERITE AND ENSTATITE

Forsterite was made by mixing stoichiometric amounts of MgO (lot EL - MgO - 6) and silicic acid, $H_2SiO_3 \cdot nH_2O$, (Fischer Certified Reagent) in the form of a water suspension. The suspension was thoroughly mixed and then dried at 110 °C until all the mechanically held water had been driven off. The mixed powder was then slowly heated up to 600 °C and held for 24 hours to drive off any remaining chemically bonded water. The resulting powder was pressed into a large compact and heated at 1350 °C for 96 hours. The sintered compact was then broken and ground into a fine powder. X - ray diffraction analysis gave excellent agreement with the reported forsterite pattern⁽⁵³⁾.

The synthesis of enstatite involved a similar procedure. Stoichiometric amounts of MgO and silicic acid were mixed in a water suspension, dried, and heated at 1350 °C for 96 hours. The diffraction pattern obtained from the product showed the presence of cristobalite, and forsterite as well as clino - enstatite. The product was then reground, thoroughly mixed, pressed into a compact and heated at 1350 °C for a further 96 hours. The regrinding procedure was repeated one more time, with a final heating at 1350 °C for 192 hours. The X - ray pattern of the product was in good agreement with the reported pattern of clino - enstatite⁽⁵⁴⁾.

APPENDIX III

DIFFRACTION PATTERN OF PROTOENSTATITE

The powder X-ray diffraction pattern of protoenstatite is given so that it may be compared with the observed X-ray patterns of the reacted samples given in Table IV-1.

ASTM Card Number 11-273Protoenstatite

d A°	I/I°	d A°	I/I°
3.24	20	1.98	20
3.17	100	1.97	20
2.91	40	1.72	13
2.73	20	1.64	20
2.55	30	1.50	15
2.31	20	1.46	15

APPENDIX IV

FURTHER THOUGHTS ON THE LACK OF ANISOTROPY OF THE REACTION AND ON THE
EXISTENCE OF AN ENSTATITE LAYER BETWEEN THE QUARTZ AND FORSTERITE PHASES

A.1 Can Enstatite Prevent Anisotropic Product Layer Growth ?

If the product layer contains two phases, enstatite as well as forsterite, the anisotropic growth effect may be reduced or eliminated. A thin layer of enstatite may exist between the major product, forsterite, and the quartz phase. The enstatite layer will be much thinner than the forsterite layer and this enstatite layer will remain at a constant relative thickness to the forsterite once local equilibrium conditions have been established at the phase boundaries. This enstatite layer will be instrumental in preventing anisotropic growth of the total product layer by causing disorientation in the original configuration of the SiO_4^{-4} lattice in the product layer, so that the forsterite orientation will bear little or no resemblance to the orientation of the quartz from whence it grew. This will prevent anisotropic growth because the reactant ions, Mg^{+2} and O^{-2} will diffuse through the forsterite at an equal rate in any direction. In the $\text{CaO} - \beta - \text{quartz}$ system, where anisotropy is observed, there is no corresponding meta - silicate layer between the quartz and Ca_2SiO_4 .

A.2 Must Enstatite Exist In The Product Layer ?

The $\text{MgO} - \text{SiO}_2$ phase diagram shows the binary compounds forsterite and enstatite to be stable at the temperatures used in this investigation, therefore barring any "non - equilibrium" effect both enstatite and forsterite

must exist in the product layer. The most probable non - equilibrium effect will be a nucleation barrier preventing the establishment of the enstatite phase. Nucleation barriers to stable phases are found in silicates whose structures involve long chains of SiO_2 repeat units. A common example of this is liquid SiO_2 failing to crystallize even on slow cooling. The long pyroxene chain structure of enstatite will similarly make nucleation of enstatite difficult. Therefore, if the nucleation of enstatite is too difficult it will not exist in the product layer.

The experimental evidence on the existence of enstatite in the product layer is inconclusive. Only one phase is evident in the product layer by metallographic examination, and this phase has been shown to be forsterite by the electron probe. An enstatite product was also not found in reaction couples made of Mg_2SiO_4 and SiO_2 after the couples had been heated at 1350°C for 24 hours. The X - ray diffraction evidence however shows that enstatite may exist. This contradicting evidence makes forming a conclusion as to whether or not enstatite exists impossible.

REFERENCES

- 1) N. L. Bowen and O. Andersen, Amer. J. of Science, 4th Ser. 38, 487, (1914).
- 2) J. W. Greig, Amer. J. of Science, 5th Ser. 13, 1, 133, (1927).
- 3) R. R. Rabston and G. T. Faust, J. Amer. Ceram. Soc. 25, 294, (1942)
- 4) W. Jander and J. Wuhrer, Z. anorg. Chem. 226, 225, (1936).
- 5) L. Degueldre, Bull. Soc. Chem. Belg. 62, 347, (1953)
- 6) G. W. Brindley and R. Hayami, Phil. Mag. 12, [117], 505, (1965).
- 7) R. Hayami and T Ogura, J. Ceram. Assoc. Japan 75, [7], (1967).
- 8) C. M. Schaudt and D. M. Roy, J. Amer. Ceram. Soc. 48, 248, (1965).
- 9) R. B. Sosman, The Phases of Silica, Rutgers University Press, New Brunswick, New Jersey, (1965).
- 10) A. L. Roberts, "Kinetics of High Temperature Processes", edited by Kingery.
- 11) W. A. Deer, R. A. Howie, and J. Zussman, Rock - Forming Minerals 4, John Wiley & Sons, Inc. New York, 180, (1963).
- 12) G. H. Beall, B. R. Korstetter, and H. L. Rittler, J. Amer. Ceram. Soc. 50, 181, (1967).
- 13) G. H. Frischat, Ber. Deut. Keram. Ges. 47, 238, (1970).
- 14) G. H. Frischat, Ber. Deut. Keram. Ges. 47, 313, (1970).
- 15) W. R. Foster, J. Amer. Ceram. Soc. 34, 255, (1951).
- 16) L. Atlas, J. Geol. 60, 125, (1952).
- 17) G. Borchardt and H. Schmalzried, Zeit. phys. Chem. N. F. 74, 265, (1971).

- 18) C. Greskovich and H. Schmalzried, J. Physics and Chem. of Solids 31, 639, (1970).
- 19) W. Plusckell, Dissertation Clausthal, (1967).
- 20) H. Schmalzried, Prog. in Solid State Chem. 2, 265, (1965).
- 21) A. M. Ginstling and B. J. Brounshtein, Zh. prikl. Khim. Mosk. 23, Engl. trans., 1327, (1950).
- 22) R. F. Carter, J. Chem. Phys. 34, 2010, 35, 1137, (1961).
- 23) R. M. Daemgen, Diplomarbeit, Clausthal, (1972).
- 24) E. F. Osborn, J. Amer. Ceram. Soc. 36, 150, (1953).
- 25) A. S. Burte and P. S. Nicholson, J. Amer. Ceram. Soc. 55, 469, (1972).
- 26) J. F. Elliott, M. Gleiser, and V. Rasakrishna, Thermochemistry for Steelmaking 2, 305, London, (1963).
- 27) W. Plusckell and H. J. Engell, Ber. Deut. Keram. Ges. 45, 388, (1968).
- 28) D. Henderson and J. Taylor, J. Iron and Steel Inst. 204, 39, (1966).
- 29) G. Rog, B. Langanke, G. Borchardt, and H. Schmalzried, yet unpublished data, communicated to Dr. Smeltzer, (1973).
- 30) C. Wagner, Z. Phys. Chem. 34, 309, (1936).
- 31) B. I. Markhasev, Izvestiya Akademii Nauk S.S.S.R. Neorganicheskie Materialy 5, 354, Engl. trans.
- 32) H. Schmalzried, Zeit. Physik. Chem. N. F. 33, 111, (1962).
- 33) H. Schmalzried, Ber. Deut. Keram. Ges. 42, 11, (1965).
- 34) J. S. Armijo, Oxid. of Metals 1, 171, (1969).
- 35) W. Gomes, Nature 192, 865, (1961).

- 36) W. Jost, Diffusion in Solids, Liquids, and Gases, p 175,
Academic Press Inc., New York.
- 37) G. Borchardt and H. Schmalzried, Ber. Deut. Keram. Ges.
49, 5, (1972).
- 38) K. Hordel and B. Strocka, Zeit. Phys. Chem N. F.
83, 234, (1973).
- 39) E. Wm. Heinrich, Microscopic Identification of Minerals, p 28,
McGraw - Hill Book Company, (1965).
- 40) Handbook of Physics and Chemistry, The Chemical Rubber
Publishing Co., (1969-70).
- 41) G. Borchardt, Diplomarbeit, Clausthal.
- 42) F. A. Cotton and G. Wilkinson, Advanced Inorganic Chemistry,
Interscience Publishers, p 461, (1966).
- 43) T. Drury, G. J. Roberts, and J. P. Roberts, "Diffusion of H₂O
in Silica Glass", Advances in Glass Technology,
Plenum Press, New York, (1962).
- 44) H. Schmalzried and C. Wagner, Z. Phys. Chem. N. F. 31, 198.
- 45) R. W. G. Wychoff, Amer. J. of Sci., ser. 5 11, 101.
- 46) P. Wei, Zeit. Krist. 92, 355.
- 47) W. L. Bragg, Atomic Structure of Minerals, Cornell
Cornell University Press.
- 48) W. L. Bragg and G. B. Brown, Zeit. Krist. 63, 538
- 49) N. Morimoto, Carnegie Inst. Washington, Ann. Rep.
Dir. Geophy. Lab., 192, (1958-59).
- 50) G. H. Frischat, Ber. Deut. Keram. Ges. 47, 364, (1970).
- 51) A. S. Burte, M. Eng. Thesis, McMaster University, (1971).

- 52) Kaichi Suito, J. of Phys. Earth 20, 225, (1972).
- 53) ASTM Card for Forsterite.
- 54) ASTM Card for Clino - enstatite.